View metadata, citation and similar papers at core.ac.uk
brought to you by CORE
provided by UPCommons. Portal del coneixement obert de la UPC

Universitat Politècnica de Catalunya

Master Thesis

Optimising fractional frequency reuse designs in MIMO networks.

Author:
Javier Atanasio Pastor Pérez

Supervisor:
Dr. Felip Riera Palou.
Juan Antonio Fernandez Rubio

A thesis submitted in fulfilment of the requirements for the degree of Master of Research on Information and Communication Technologies (MERIT)

in the

Research Group Name
Department of Teoria del Senyal i Comunicacions

December 2014

UNIVERSITAT POLITECNICA DE CATALUNYA (UPC)

Abstract

Escola Tècnica Superior d'Enginyeria de Telecomunicació de Barcelona
Department of Teoria del Senyal i Comunicacions

Master of Research on Information and Communication Technologies (MERIT)

Optimising fractional frequency reuse designs in MIMO networks.

by Javier Atanasio Pastor Pérez

Fractional frequency reuse (FFR) is an interference cancellation technique that has become increasingly popular in the context of 4G systems. The combination of FFR with advanced multiple-antenna technology in the form of multiuser MIMO (MU-MIMO) and base station cooperation using coordinated multipoint transmission (CoMP), paves the way to realize the ambitious goals in terms of area spectral efficiency contemplated within LTE-A. This work explores various architectures combining the use of FFR and advanced MIMO procesing (MU-MIMO, CoMP). Single -antenna and multiple-antenna configurations at each communicating end have been considered. An abstraction of the physical layer of the proposed system is provided in the form of SINR expressions that can then be used to derive optimal values for different parameters, most notably, those affecting the FFR configuration such as the threshold radius delimiting the central and edge areas of the cell.

Acknowledgements

I would like to express my deep gratitude to Professor Guillem Femenias Nadal and Professor Felip Riera Palou, my research supervisors, for their patient guidance, enthusiastic encouragement and useful critiques of this research work. I would also like to thank Professor Juan Antonio Fernandez Rubio, for her advice and assistance.

I wish to thank my parents for their support and encouragement throughout my study and finally to Haizea Llorente Onaindia for her unconditional support.

Contents

List of Figures

List of Tables

Chapter 1

Introduction

1.1 Introduction

Fractional frequency reuse (FFR), multiple antenna technology (MIMO) and coordinated multipoint (CoMP) transmission working on a physical layer based on orthogonal frequency division multiple access (OFDMA) are expected to play a fundamental role in achieving the ambitious throughput requirements considered within the Third Generation Partnership Project Long-Term Evolution-Advanced (3-GPP's LTE-A) [1]. Moreover, these mechanisms are envisaged to be at the core of the next generation of wireless communications, so-called 5G systems.

Typically, in FFR-based cellular systems, a low frequency reuse factor is chosen for the cell-center users, less affected by cochannel interference, and a larger frequency reuse factor is chosen for the cell-edge users, more prone to strong inter-cell interference. In order to maximize the overall area spectral efficiency, the reuse factor at the cell edge, the parameters defining the cell centre and edge regions and the spectrum allocation to centre and edge, must be carefully designed to strike a balance between maximising frequency reuse while minimising intercell interference. Depending on whether the FFR pattern changes with time or not, dynamic or static FFR schemes can be defined. Analytical performance studies of static FFR schemes are presented in [2] and [3]. In particular, throughput expressions and the optimal distance threshold that is used to distinguish between the cell-center and cell-edge users are derived in [2] considering a

cellular OFDMA-based network made of circular cells. In [3] a new analytical framework used to evaluate coverage probability and average rate in FFR systems leading to tractable expressions is presented assuming the base station deployment follows a Poisson point process. Nevertheless, these studies neglect the use of sectorization, which is typically found in most practical deployments. Aiming at further increasing network capacity, interference cancellation through base station cooperation (CoMP) [4] can complement the use of an interference coordination technique such as FFR. Essentially, in a CoMP system different BSs cooperate to transmit signals to a set of users transforming in this way the potential inter-cell interference (ICI) into useful signal. Multiuser MIMO (MU-MIMO) techniques like Block Diagonalization (BD) [5], Zero-forcing Beamforming (ZF-BF) and Zero-forcing Dirty Paper Coding (ZF-DPC) [6] are employed for this purpose. All of them require of a perfect synchronization among the cooperating BSs and a robust backhaul network but, as it will be shown later, each MU-MIMO technique has different requirements in terms of signal processing complexity and amount of information to be shared among cooperating base stations.

Both techniques, CoMP and FFR, have been extensively treated, mostly on a separate basis, in the literature in the context of OFDMA networks [7]-[8]. In [7], an analysis of the inter-cell interference coordination in multicellular OFDMA system is provided, determining the optimal frequency reuse factor of the exterior users as well as the bandwidth to assign to both interior and exterior zones. In [9] cooperative communication technologies being considered within LTE-A are compared. Nevertheless no study is available that jointly considers the effects of both mechanisms, a crucial aspect, given their close interaction. This work aims at filling in this gap by defining a common framework in which different CoMP and FFR strategies can be assessed and compared.

We start with a simple SISO configuration and continue by allowing multiple antennas at each communication end. This generalization is far from trivial, as the possibility of MIMO processing at both ends, opens a vast array of possibilities, some of them resulting in prohibitive computational complexity. Consequently, suboptimal strategies based on greedy principles are proposed in this report that strive to reap the benefits MIMO architectures offer, while remaining computationally feasible. In particular, it will be shown that a block diagonalization-based scheme, suitably adapted to the considered setup, results in near-optimal performance at a reasonable computational cost with potential to be practically deployed. To this end, SINR expressions for the proposed

system are derived that serve as a characterization of the physical layer. Furthermore, a critical parameter for the FFR component of the system, namely, the threshold radius separating the edge and centre regions, is thoroughly investigated.

1.2 Publications

The work contained in this thesis has resulted in the following publications:

- "Combining fractional frequency reuse with coordinated multipoint transmission in MIMO-OFDMA networks," Wireless Days (WD), 2013 IFIP , vol., no., pp.1,8, 13-15 Nov. 2013.
- "FFR-aided coordinated multipoint transmission in downlink multicell MIMO-OFDMA networks" (submitted).

1.3 Thesis Structure

The rest of this Thesis is organized as follows. Chapter 2 introduces a systematic comparative study combining FFR and CoMP techniques with a simplified system model and with the limitation of one antenna per BS and MS (i.e., SISO configurations). In Chapter 3 we allow multiple antennas at BS and MS, thus allowing the use of more complex CoMP techniques with a new more realistic environment. Finally the main results of this work are recapped in Chapter 5 and directions for further work are provided.

Chapter 2

FFR design in network MIMO: Single antenna scenarios

2.1 System model

A downlink MU-MIMO cellular system based on OFDMA with 19 cells (one center cell and two tiers of neighbouring cells) is considered. Each cell is divided into four regions. The center region is defined by a circular area of radius R_{th} and cell-centre users are served by M_C omnidirectional antennas. In the edge of the cell, three 120^o sectors are defined, each served by M_E sectorial antennas. The BS antennas are co-located and a uniform power P_{sc} is allocated per subcarrier. The total bandwidth is split into two bands, B_C and B_E, allocated to cell center and cell edge areas, respectively. Furthermore, the cell edge bandwidth B_E is divided into three equal subbands, namely, B_{E_1}, B_{E_2} and B_{E_3}. The frequency distribution among cell-edge sectors depends on the transmission scheme employed. In the regular distribution, used in non-cooperative schemes, (Fig. 2.2b) all the sectors with the same main-beam direction are allocated the same frequency band. In the rearranged distribution, used in cooperative schemes, sectors pointing towards the same area are allocated the same frequency band. Those sectors are organized in clusters. A cluster is formed by three neighbour sector BSs working in a cooperative way on the same frequency subband (Fig. 2.2c). Thus, assuming a subcarrier bandwidth equal to Δf, and given a total bandwidth B, the system has

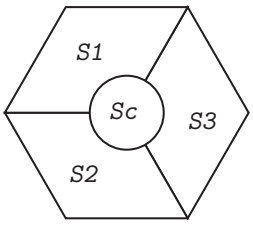

Sc: Center Sector
S1: Edge Sector 1
S2: Edge Sector 2
S3: Edge Sector 3

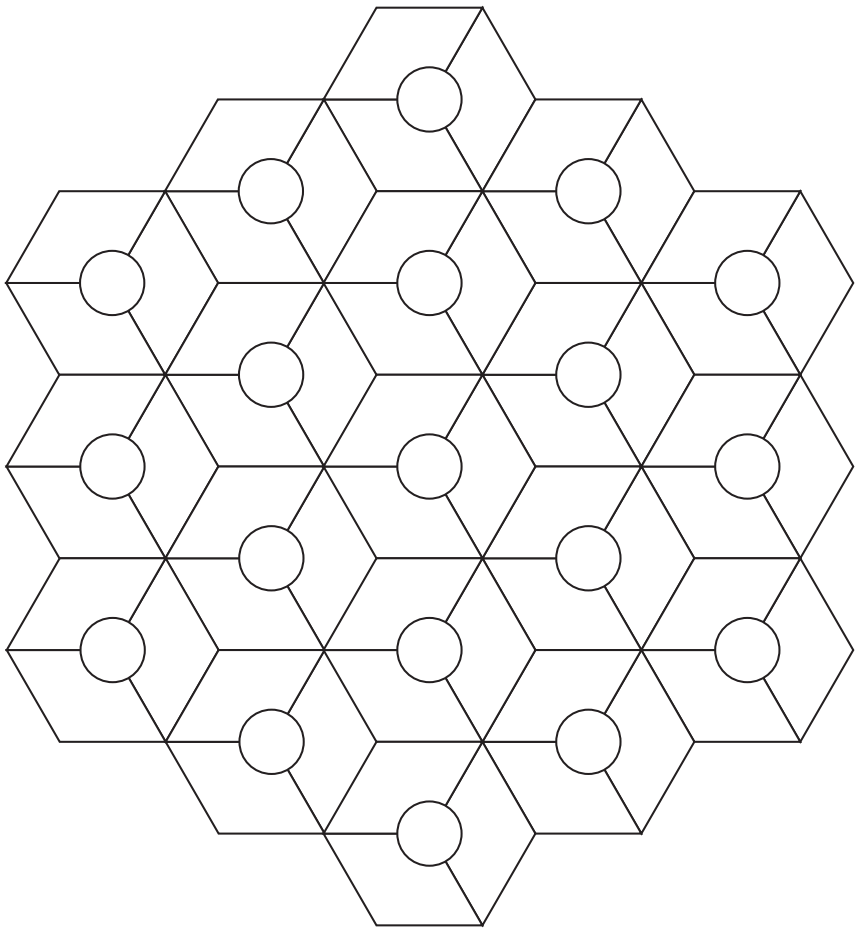

FIGURE 2.1: 19-cell Network.

$N_{SC} = B/\Delta f$ subcarriers, out of which $N_{SC}^{c} = B_C/\Delta f$ are allocated to the center region and $N_{SC}^{e} = B_{E_i}/\Delta f$ to each of the edge sectors.

A total of N_u users, each with $N_R = 1$ antennas, are uniformly distributed in each sector. If the distance between a user and its closest BS is smaller than R_{th}, the user is deemed to belong to the cell-center. The rest of users are considered to belong to the cell-edge.

The channel response linking an arbitrary antenna j from BS s and antenna i from a generic user u on an arbitrary subcarrier is modelled as

$$h_{s,u}^{i,j} = \alpha_{s,u}^{i,j} \sqrt{\beta_{s,u} A(\theta_{s,u}^{i,j}) d_{s,u}^{-\mu} \Gamma} \tag{2.1}$$

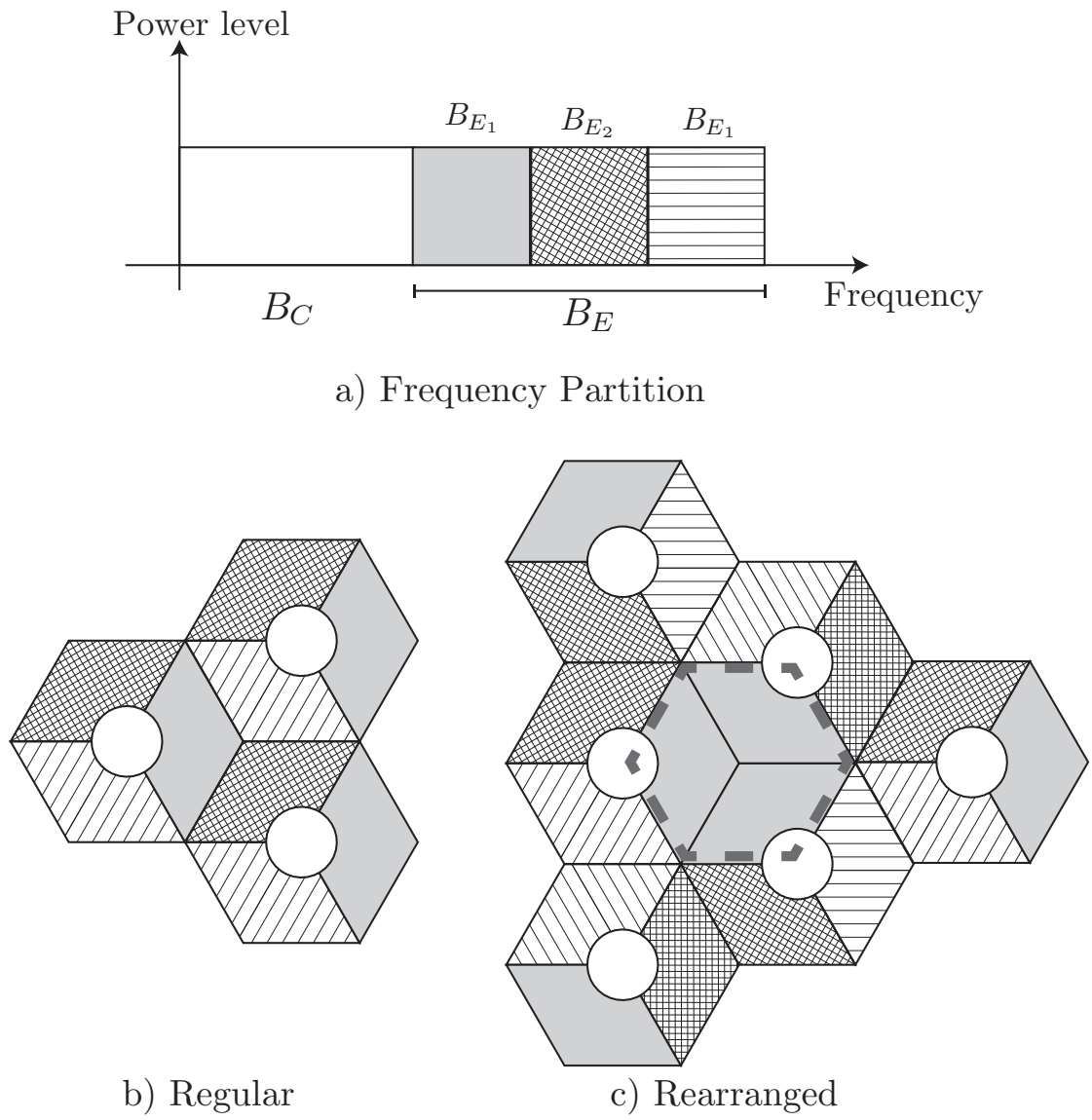

FIGURE 2.2: Frequency Partition.

where $\alpha^u_{s,i,j}$ and β^u_s are the fast Rayleigh fading and shadowing respectively; $A(\theta^u_{s,i,j})$ is the antenna gain pattern at angle $\theta^u_{s,i,j} \in [-180°, 180°]$, representing the pointing angle between antenna j from BS s and user antenna i with respect to the main-beam direction of the considered antenna; $d_{s,u}$ is the distance between BS s and user u; μ is the path loss exponent and Γ is a constant parameter capturing the effect of various channel and system parameters including cable losses, carrier frequency, antenna heights, maximum antenna gains, and other link budget parameters [8].

The gain pattern used for each sector antenna is defined as [8]

$$A(\theta)_{dB} = \begin{cases} 0 & \text{omnidirectional} \\ -\min\left[12\left(\frac{\theta}{\theta_{3dB}}\right)^2, A_m\right] & \text{sectorial} \end{cases} \tag{2.2}$$

where $\theta_{3dB} = 70^o$ is the angle at which the antenna gain is 3 dB lower than the antenna gain at the main-beam direction, and the parameter $A_m = 20\ dB$ is the maximum attenuation measured at the sidelobe.

2.2 PHY-Layer characterization

This section derives analytical expressions characterizing the physical layer of the considered scheme for both cell center and cell edge. To compute the capacity values of the different architectures, SINRs expressions are necessary, and these can be derived from the corresponding reception equations.

2.2.1 Cell-center users

Cell-center users all rely on conventional single-input single-output (SISO) transmission. Assuming that a cell-center user u connected to BS s has been allocated subcarrier n, the received signal is given by

$$y_{s,u}[n] = \underbrace{P_{sc} h_{s,u}[n] s_{s,u}[n]}_{\text{desired signal}} + \underbrace{\sum_{s' \neq s} P_{sc} h_{s',u}[n] s_{s',u'}[n]}_{\text{interference}} + \underbrace{\eta_{s,u}[n]}_{\text{noise}}, \tag{2.3}$$

where $s_{s,u}[n]$ is the normalized symbol (energy equal to 1) transmitted by BS s to the selected user u on subcarrier n; $h_{s,u}$, conforming to (2.1), denotes the channel between BS s and user u, where the superindex is omitted because there is only one antenna at each end and $\eta_{s,u}[n]$ is a sample of a circularly symmetric zero-mean additive white Gaussian noise with variance σ_η^2.

Using (2.3), the SINR for user u connected to BS j on subcarrier n can be expressed as

$$\gamma^C_{s,u}[n] = \frac{P_{sc}|h_{s,u}[n]|^2}{\sigma^2_\eta + \sum\limits_{s' \neq s} P_{sc}|h_{s',u}[n]|^2}. \tag{2.4}$$

2.2.2 Cell-edge users

Cell-edge users are served relying on some form of BS cooperation. To this end, let us denote by $\mathcal{B}[n]$ the set of sectors transmitting on subcarrier n that can be organized in clusters[1]. In this report, each cluster has three sectors BSs. Sector BSs $\mathcal{B}_{c'}[n]$ in cluster c' cooperate to transmit to a set of users $\mathcal{U}_{c'}[n]$ in the sectors they cover. The signal transmitted by sector BS $b' \in \mathcal{B}_{c'}[n]$ can be expressed as

$$x_{c',b'}[n] = \mathbf{w}^T_{c',b'}[n]\mathbf{s}_{c'}[n], \tag{2.5}$$

where $\mathbf{w}_{c',b'}[n] \in \mathbb{C}^{|\mathcal{U}_{c'}[n]|\times 1}$ is the weighting vector used to transmit the vector of normalized symbols $\mathbf{s}_{c'}[n] \in \mathbb{C}^{|\mathcal{U}_{c'}[n]|\times 1}$ to the set of users $\mathcal{U}_{c'}[n]$ that are cooperatively served by the sector BSs in set $\mathcal{B}_{c'}[n]$, with $\|\boldsymbol{w}_{c',b'}[n]\|^2 \leq P_{sc}$ (per subcarrier power constraint). The signal vector transmitted by these BSs can then be expressed as

$$\mathbf{x}_{c'}[n] = \mathbf{W}_{c'}[n]\mathbf{s}_{c'}[n] = \begin{bmatrix} \mathbf{w}^T_{c',1}[n] \\ \vdots \\ \mathbf{w}^T_{c',|\mathcal{B}_{c'}[n]|}[n] \end{bmatrix} \mathbf{s}_{c'}[n], \tag{2.6}$$

where $|\mathcal{B}_{c'}|$ is the number of sector BSs cooperating in cluster c'. Note that depending on the design of $\boldsymbol{W}_{c'}[n]$ (see Section 2.5.3 (page 20)), the cooperating BSs will need to share their channel state information (CSI).

The composed vector of the signals received by the set of users in $\mathcal{U}_c[n]$, that is, the set of users in cluster c that are cooperatively served by sector BSs in $\mathcal{B}_c[n]$, is given by

$$\mathbf{y}_c[n] = \sum_{\forall c'} \mathbf{H}_{c',c}[n]\mathbf{x}_{c'}[n] + \eta_c[n] = \sum_{\forall c'} \mathbf{H}_{c',c}[n]\mathbf{W}_{c'}[n]\mathbf{s}_{c'}[n] + \eta_c[n], \tag{2.7}$$

[1] Although the proposed framework applies to any cluster configuration, cluster formation strategies are out of the scope of this work and, thus, except otherwise stated, it will be assumed throughout this work that, as shown in Fig. 2.2, (dotted lines), clusters contain only three sector BSs and are organized either in a regular or a rearranged distribution

where $\mathbf{H}_{c',c}[n] \in \mathbb{C}^{|\mathcal{U}_c[n]|\times|\mathcal{B}_{c'}[n]|}$ is the MIMO channel matrix between transmitting sector BSs in cluster c' and the receiving antennas of the set of users cooperatively served by sector BSs in cluster c, defined by

$$\mathbf{H}_{c',c}[n] = \begin{bmatrix} \mathbf{h}_{c',c,1}[n] \\ \vdots \\ \mathbf{h}_{c',c,|\mathcal{U}_c[n]|}[n] \end{bmatrix},$$

with $\mathbf{h}_{c',c,u}[n] \in \mathbb{C}^{1\times|\mathcal{B}_{c'}[n]|}$ representing the channel vector between transmitting sector BSs in cluster c' and the receiving antenna of user $u \in \mathcal{U}_c[n]$.

The signal received by user u in cluster c can then be written as

$$\begin{aligned} y_{c,u}[n] &= \sum_{\forall c'} \mathbf{h}^T_{c',c,u}[n]\mathbf{x}_{c'}[n] + \eta_{c,u}[n]\sum_{\forall c'} \mathbf{h}^T_{c',c,u}[n]\mathbf{W}_{c'}[n]\mathbf{s}_{c'}[n] + \eta_c[n] \\ &= \underbrace{\mathbf{h}^T_{c,c,u}[n]\mathbf{w}_{c,u}[n]s_{c,u}[n]}_{\text{desired signal}} + \underbrace{\mathbf{h}^T_{c,c,u}[n]\mathbf{W}_{c,\overline{u}}[n]\mathbf{s}_{c,\overline{u}}[n]}_{\text{intra-cluster interference}} \\ &+ \underbrace{\sum_{\forall c',c'\neq c} \mathbf{h}^T_{c',c,u}[n]\mathbf{W}_{c'}[n]\mathbf{s}_{c'}[n]}_{\text{inter-cluster interference}} + \eta_c[n], \end{aligned} \tag{2.8}$$

where $\mathbf{W}_{c,\overline{u}}[n]$ denotes matrix $\mathbf{W}_c[n]$ with the u^{th} row removed and, similarly, $\mathbf{s}_{c,\overline{u}}[n]$ corresponds to vector $\mathbf{s}_c[n]$ with the u^{th} element removed.

2.2.2.1 Uncoordinated SISO Scheme

In this case there is no coordination among BSs, the transmission scheme is identical to that used to serve the cell-center users, but the cellular system is sectorized (note that in this uncoordinated scheme clusters consist of a single sector BS). The SINR can then be expressed as in (2.4) but, in this case, the channel response contains the gain of a sectorial BS antenna. Recall also that, in this case, the frequency planning used in the one shown in figure 3.2 b).

2.2.2.2 Coordinated Single-User Joint Transmission (SU-JT)

Here, the set of sector BSs in a cluster cooperate to transmit to a single user in their coverage area. Cooperating sector BSs in cluster c use the SINR-maximizing weighting

vector

$$\mathbf{w}_{c,u}[n] = \left[\begin{array}{ccc} \frac{h^*_{c,1,c,u}[n]}{|h_{c,1,c,u}[n]|} & \cdots & \frac{h^*_{c,|\mathcal{B}_c[n]|,c,u}[n]}{|h_{c,|\mathcal{B}_c[n]|,c,u}[n]|} \end{array} \right]^T \tag{2.9}$$

to transmit symbol $s_{c,u}[n]$ to user u. As transmission is directed to a single user within the cluster, there is no intra-cluster interference, that is, $\mathbf{W}_c[n] = \mathbf{w}_{c,u}[n]$. Thus, the signal received by user u in cluster c can be expressed as

$$\begin{aligned} y^{SU-JT}_{c,u}[n] = & \underbrace{s_{c,u}[n] \sum_{b=1}^{|\mathcal{B}_c[n]|} |h_{c,b,c,u}[n]|}_{\text{desired signal}} \\ & + \underbrace{\sum_{\forall c' \neq c} s_{c',u'}[n] \sum_{b'=1}^{|\mathcal{B}_{c'}[n]|} h_{c',b',c,u}[n] \overbrace{\frac{h^*_{c',b',c',u'}[n]}{|h_{c',b',c',u'}[n]|}}^{w_{c',b',c',u'}[n]}}_{\text{inter-cluster interference}} \\ & + \eta_{c,u}[n] \end{aligned} \tag{2.10}$$

and the corresponding SINR is

$$\gamma^{SU-JT}_{c,u}[n] = \frac{P_{sc} \left(\sum_{b=1}^{|\mathcal{B}_c[n]|} |h_{c,b,c,u}[n]| \right)^2}{\sigma^2_\eta + P_{sc} \sum_{\forall c' \neq c} \sum_{b'=1}^{|\mathcal{B}_{c'}[n]|} |h_{c',b',c,u}[n] w_{c',b',c',u'}[n]|^2}. \tag{2.11}$$

2.2.2.3 Zero-Forcing

Now, let us asume that the $|\mathcal{B}_{c'}[n]|$ sector BSs in cluster c' cooperate to transmit to the $|\mathcal{U}_{c'}[n]| \leq |\mathcal{B}_{c'}[n]|$ users in $\mathcal{U}_{c'}[n]$ with the goal of eliminating the intra-cluster interference while simultaneously fullfilling the per sub-carrier power constraints. This can be accomplished by using a transmit filter equal to the Moore-Penrose pseudoinverse of the channel matrix $\mathbf{H}_{c',c'}[n]$ weighted by a power allocation matrix $\mathbf{G}_{c'}[n]$ that guarantees the per-subcarrier power constraints. That is,

$$\begin{aligned} \mathbf{W}_{c'}[n] &= \mathbf{H}^\dagger_{c',c'}[n] \mathbf{G}_{c'}[n] \\ &= \underbrace{\mathbf{H}^H_{c',c'}[n] \left(\mathbf{H}_{c',c'}[n] \mathbf{H}^H_{c',c'}[n] \right)^{-1}}_{\mathbf{F}_{c'}[n]} \mathbf{G}_{c'}[n] \end{aligned} \tag{2.12}$$

Algorithm 1 : Power Management.

(a) Define $\mathbf{R}_{c'}[n] = [r_{c'_{b',u'}}]_{|\mathcal{B}_{c'}[n]|\times|\mathcal{U}_{c'}[n]|}$, such that $r_{c'_{b',u'}} = |f_{c'_{b',u'}}|^2$

(b) Solve the system of linear equations:

$$\mathbf{R}_{c'}[n] \begin{bmatrix} g^2_{c',1}[n] \\ \vdots \\ g^2_{c',|\mathcal{U}_{c'}[n]|}[n] \end{bmatrix} = \begin{bmatrix} P_{sc} \\ \vdots \\ P_{sc} \end{bmatrix}$$

(c) Check solutions

if $g_{c',u'}[n] \geq 0, \forall u'$ **then**

the solution is valid

else

the solution is not valid and we use the normalization

$$g_{c',u'}[n] = \sqrt{\frac{P_{sc}}{\max_u [\mathbf{F}_{c'}[n]\mathbf{F}_{c'}[n]^H]_{u,u}}}$$

end if

where

$$\mathbf{G}_{c'}[n] = \mathcal{D}\left(\begin{bmatrix} g_{c',1}[n] & \dots & g_{c',|\mathcal{U}_{c'}[n]|}[n] \end{bmatrix} \right)$$

with $\mathcal{D}(\mathbf{x})$ denoting a diagonal matrix with vector $\mathbf{x}$ at its main diagonal. For convenience, $\mathbf{F}_{c'}[n]$ is explicitly defined as

$$\mathbf{F}_{c'}[n] = \begin{bmatrix} f_{c'_{1,1}} & \dots & f_{c'_{1,|\mathcal{U}_{c'}[n]|}} \\ \vdots & \ddots & \vdots \\ f_{c'_{|\mathcal{B}_{c'}[n]|,1}} & \dots & f_{c'_{|\mathcal{B}_{c'}[n]|,|\mathcal{U}_{c'}[n]|}} \end{bmatrix}.$$

Using this transmit filter, the signal received by user u in cluster c can be written as:

$$\begin{aligned} y^{ZF}_{c,u}[n] =& g_{c,u}[n]s_{c,u}[n] \\ &+ \sum_{\forall c' \neq c} \sum_{u'=1}^{|\mathcal{U}_{c'}[n]|} g_{c',u'}[n]s_{c',u'}[n] \sum_{b'=1}^{|\mathcal{B}_{c'}[n]|} h_{c',b',c,u}[n] f_{c'_{b',u'}}[n] + \eta_{c,u}[n]. \end{aligned} \tag{2.13}$$

The use of ZF precoding may limit the utilization of the maximum power available at each BS as this could result in the violation of the per-subcarrier power constraint. In order to address this problem, Algorithm 1 is proposed. This algorithm first attempts to use all available transmit power and, upon detection of the power constraint violation, a normalization is applied to restore it. This normalization factor is computed targetting the maximization of the minimum rate among the coordinated sectors [10].

Based on (2.13), the SINR of user u in cluster c is found to be

$$\gamma_{c,u}^{ZF}[n] = \frac{|g_{c,u}[n]|^2}{\sigma_\eta^2 + \sum\limits_{\forall c' \neq c} \sum\limits_{u'=1}^{|\mathcal{U}_{c'}[n]|} \sum\limits_{b'=1}^{|\mathcal{B}_{c'}[n]|} |g_{c',u'}[n] h_{c',b',c,u}[n] f_{c'_{b',u'}}[n]|^2}. \tag{2.14}$$

2.2.2.4 Zero-Forcing Dirty Paper Coding

The QR decomposition of channel matrix $\mathbf{H}_{c'}[n]$ can be expressed as $\mathbf{H}_{c'}[n] = \mathbf{L}_{c'}[n]\mathbf{Q}_{c'}[n]$, where $\mathbf{L_{c'}[n]}$ is a lower triangular matrix with (u', b')-th entry $l_{u',b'}$, and $\mathbf{Q}_{c'}[n]$ is a unitary matrix with $\mathbf{Q}_{c'}[n]\mathbf{Q}_{c'}^H[n] = \boldsymbol{I}_{|\mathcal{U}_{c'}[n]|}$. By constructing the linear weighting matrix $\mathbf{W}_{c'}[n] = P_{sc}\mathbf{Q}_{c'}^H[n]$, the received signal for user u in cluster c can be written as

$$\begin{aligned} y_{c,u}^{ZFDPC}[n] = & \underbrace{P_{sc} l_{c_{u,u}}[n] s_{c,u}[n]}_{\text{desired signal}} \\ & + \underbrace{P_{sc} \sum_{i<u} l_{c_{u,i}} s_{c,i}[n]}_{\text{(non-causal) intra-cluster interference}} \\ & + \underbrace{P_{sc} \sum_{\forall c' \neq c} \sum_{u'=1}^{|\mathcal{U}_{c'}[n]|} s_{c',u'}[n] \sum_{b'=1}^{|\mathcal{B}_{c'}[n]|} h_{c',b',c,u}[n] w_{c'_{b',u'}}[n]}_{\text{inter-cluster interference}} \\ & + \eta_{c,u}[n]. \end{aligned} \tag{2.15}$$

That is, the use of $\mathbf{W}_{c'}[n] = P_{sc}\mathbf{Q}_{c'}^H[n]$ forces to zero the intra-cluster interference from data symbols $s_{c,i}$ with $i > u$. Furthermore, due to unitarity of $\mathbf{Q}_{c'}[n]$, the use of this weighting matrix allows the fulfillment of the per-subcarrier power constraints with equality. The rest of intra-cluster interference produced by symbols $s_{c,i}$ with $i < u$, called non-causal interference, can now be eliminated by successive interference cancellation or DPC. Assuming the use of DPC at the transmitter side, the equivalent received signal

can finally be expressed as

$$\begin{aligned} y_{c,u}^{ZFDPC}[n] = & \underbrace{P_{sc} l_{c_{u,u}}[n] s_{c,u}[n]}_{\text{desired signal}} \\ & + \underbrace{P_{sc} \sum_{\forall c' \neq c} \sum_{u'=1}^{|\mathcal{U}_{c'}[n]|} s_{c',u'}[n] \sum_{b'=1}^{|\mathcal{B}_{c'}[n]|} h_{c',b',c,u}[n] w_{c'_{b',u'}}[n]}_{\text{inter-cluster interference}} \\ & + \eta_{c,u}[n]. \end{aligned} \tag{2.16}$$

The SINR of user u in cluster c is then given by

$$\gamma_{c,u}^{ZFDPC}[n] = \frac{P_{sc} |l_{c_{u,u}}[n]|^2}{\sigma_\eta^2 + P_{sc} \sum_{\forall c' \neq c} \sum_{u'=1}^{|\mathcal{U}_{c'}[n]|} \sum_{b'=1}^{|\mathcal{B}_{c'}[n]|} |h_{c',b',c,u}[n] w_{c'_{b',u'}}[n]|^2}. \tag{2.17}$$

2.3 Cell-capacity

The instantaneous capacity of cell j can be obtained by considering the multicarrier nature of the OFDMA system and adding up the capacities of all the transmission channels established by the system to users in the area of cell j. In this way, the instantaneous capacity allocated to cell-center users served by BS j can be written as

$$C_j^{center} = \Delta f \sum_{\forall n \in \mathcal{N}^{center}} \log_2(1 + \gamma_{u,j}[n]) \tag{2.18}$$

where we have assumed that the scheduling and user selection algorithms have allocated subcarriers in set $\mathcal{N}^{center}$ to served users. By defining $\mathcal{C}_j$ as the set of clusters containing a sector covered by cell j, and by $\mathcal{U}_{j,c}$ the set of users in cluster c located in the area of cell j, the instantaneous capacity allocated to cell-edge users served by BS j can be written as

$$C_j^{edge} = \Delta f \sum_{\forall c \in \mathcal{C}_j} \sum_{\forall u \in \mathcal{U}_{j,c}} \sum_{\forall n \in \mathcal{N}_c^{edge}} \log_2(1 + \gamma_{c,u}[n]), \tag{2.19}$$

where, once again, we have assumed that the scheduling and user selection algorithms have allocated subcarriers in set $\mathcal{N}_c^{edge}$ to users in cluster c. Obviously, the total instantaneous capacity of cell j can be obtained as

$$C_j = C_j^{center} + C_j^{edge}. \tag{2.20}$$

The ergodic (average) capacity can be obtained by averaging (either analytically or using Monte Carlo repeated random numerical experiments) the instantaneous capacity over system parameters such as the spatial distribution of users, the fast Rayleigh fading, the shadowing, or the subcarrier allocation strategy.

2.4 User selection

Two different scheduling strategies, round robin (RR) and maximum SINR (MSINR), have been considered. In RR, the users in cluster c allocated to subcarrier n are randomly selected, with equal probability, from the set of users $\mathcal{U}_c[n]$. This strategy guarantees maximum fairness (in terms of radio resources) among multiple users at the cost of totally neglecting the potential multiuser diversity gain. In contrast, MSINR scheduling exploits multiuser diversity by selecting users with the maximum SINR on each subcarrier, that is,

$$u_{MSINR} = \arg \max_{u \in \mathcal{U}_c[n]} \{\gamma_{c,u}[n]\}. \tag{2.21}$$

Note that the solution of (2.21) for non-cooperating or SU-JT transmission schemes is rather trivial. In contrast, for ZF and ZF-DPC, $|\mathcal{B}_c[n]|$ user combinations should be formed, and therefore, the computation of (2.21) necessarily implies the evaluation of the SINR for all possible user groupings and orderings. Such exhaustive search is prohibitive even for moderate number of users. Consequently, suboptimal strategies such as the one introduced in [11] are required. This user selection method relies on a greedy heuristic to determine an approximate solution of (2.21).

Note that any scheduling algorithm will typically be evaluated with respect to two, often conflicting, performance metrics, namely, capacity and fairness. While MSINR is the optimum scheduler from the point of view of maximising the former, it totally neglects the latter. In contrast, RR will lead to a perfectly equitative sharing of the radio resources at the cost of sacrificing capacity. In fact, MSINR and RR represent the

TABLE 2.1: Simulation parameters

Parameters	Values
Number of cells	19
Number of sectors per cluster	3
Maximum transmit power per sector	30 Watts
Number of users per sector	N_u
Number of receive antennas per user	1
Number of subcarriers	$N = 512$
Subcarriers for cell-edge users	$N_{edge} = 85$
Subcarriers for cell-center users	$N_{center} = 257$
Subcarrier bandwidth	$\Delta f = 15kHz$
BS-to-BS distance	2 Km
Standard deviation of shadowing	$\sigma_\beta = 8dB$
Path loss exponent	$\mu = 4$

two extreme strategies in the capacity *vs* fairness plane, with any other strategy (e.g. proportional fairness) lying somewhere in the middle.

2.5 Simulation results

An OFDMA network with $N_c = 19$ cells is considered where up to three sector BSs cooperate to transmit to users in the cell edge. Thus, clusters consist of $|\mathcal{B}_c[n]| = 3$ sector BSs. The parameter $\Gamma/\sigma_\eta^2 = -43.25$ dB for a BS-to-BS distance of 2 km. Table 2.1 summarizes the rest of simulations parameters, most of them extracted from [2], [8] and in line with current 4G specifications such as those found in LTE.

2.5.1 Optimal Threshold Radius

A major design decision in any FFR-based system is the definition of the center and edge areas. To this end, it is important to evaluate the impact the threshold radius R_{th} has on the performance of the different CoMP schemes. Figure 2.3 shows the capacity of cell center users as a function of R_{th} with number of users as parameter when using both MSINR scheduling (upper plot) and Round Robin scheduling (lower plot). Note that only SISO transmission is evaluated in this case since cell-center users are not served in a coordinated fashion. These results reveal that if a small radius is chosen, the probability of not having any cell-center user increases, thus wasting resources allocated to the cell-center area as these subcarriers will remain unassigned. In contrast, if a large

TABLE 2.2: Mean SINR

	FFR Schemes					Non-FFR Schemes	
Scheme	Cell-center	ZF-DPC	ZF	SU-JT	SISO	1-sector	3-sector
RR	35.55 dB	17.53 dB	11.56 dB	22.61 dB	9.19 dB	2.63 dB	10.06 dB
MSINR	44.11 dB	27.93 dB	26.32 dB	43.99 dB	11.19 dB	44.51 dB	16.13 dB

radius is chosen, cell-center users close to the cell-edge area are likely to suffer from large inter-cell interference. This effect can be appreciated when using RR as in this case these borderline users are still scheduled for transmission, thus lowering the average capacity (MSINR will almost completely neglect these users).

Figure 2.4 depicts the cell-edge users mean capacity when using different CoMP schemes for $N_u = 30$ users (MSINR in the upper plot and RR in the lower plot). If a large radius is chosen, the probability that there are no cell-edge users increases, thus decreasing the corresponding capacity. On the contrary, a small radius almost guarantees the existence of cell-edge users, thus avoiding any waste of resources. Note that regardless the scheduling policy, DPC-ZF clearly outperforms the rest of CoMP schemes. ZF precoding performance comes close to that of DPC-ZF under MSINR scheduling and thus can be considered as an attractive solution showing a good trade-off between performance and complexity. Nevertheless, the radius selection should be done taking into account both cell-center and cell-edge users. To this end, figure 2.5 shows how the overall mean capacity varies as a function of the radius when using different transmission schemes and different schedulers when there are $N_u = 30$ users per sector. Remarkably, the overall optimum radius is within a rather narrow range (150-230 m) for any CoMP technique or scheduling policy. It is envisaged that optimum radius for other schedulers (e.g. proportional fairness) are most likely to be also in this range.

For the ZF results shown in figure 2.4, the power allocation scheme adopted is the one defined by Algorithm 1 in Section IV.B. In order to illustrate the clear advantage of this proposal in comparison to the conventional power allocation (see, for example, [8]), figure 2.7 shows average capacity results for both strategies as a function of R_{th} and with $N_u = 30$. As can be observed, the proposed power allocation method provides a capacity advantage of up to 1.5 bps/Hz for the radius that are most likely to be used in practical systems.

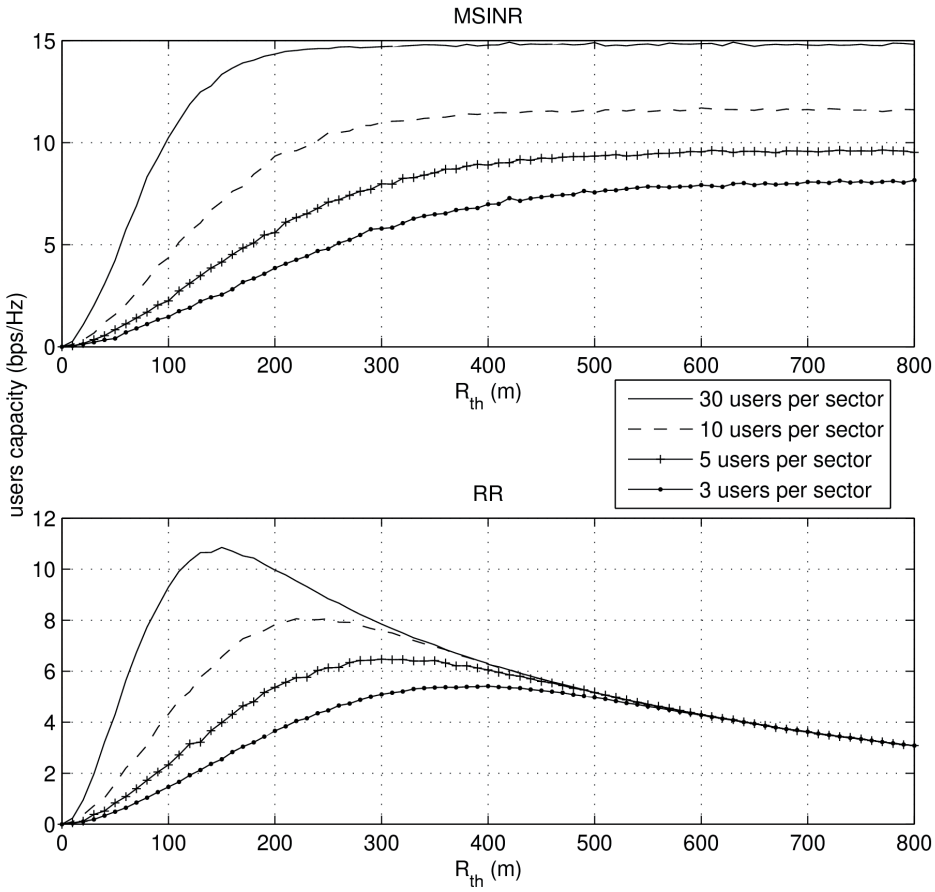

FIGURE 2.3: Cell-center users capacity.

TABLE 2.3: Mean Cell Capacity (bps/Hz)

	FFR Schemes					Non-FFR Schemes	
Scheme	Cell-center	ZF-DPC	ZF	SU-JT	SISO	1-sector	3-sector
RR	10.83	6.07	4.36	2.58	3.91	2.58	4.17
MSINR	14.63	9.29	8.76	4.87	4.40	14.79	5.97

2.5.2 SINR and Capacity

Concentrating now on the optimum radius settings, $R_{th} = 150$ m and $R_{th} = 230$ m for RR and MSINR, respectively, and $N_u = 30$ users/sector, we investigate the mean SINR for the different CoMP schemes that have considered in this paper. Table 2.3 collects the mean SINR for cell-center and cell-edge users. For comparative purposes, results obtained for systems without FFR are also included. In particular, reuse one with omnidirectional antennas and reuse 3 with trisectorial antennas are considered. It can be observed that cell-center users using FFR exhibit higher SINR values, due

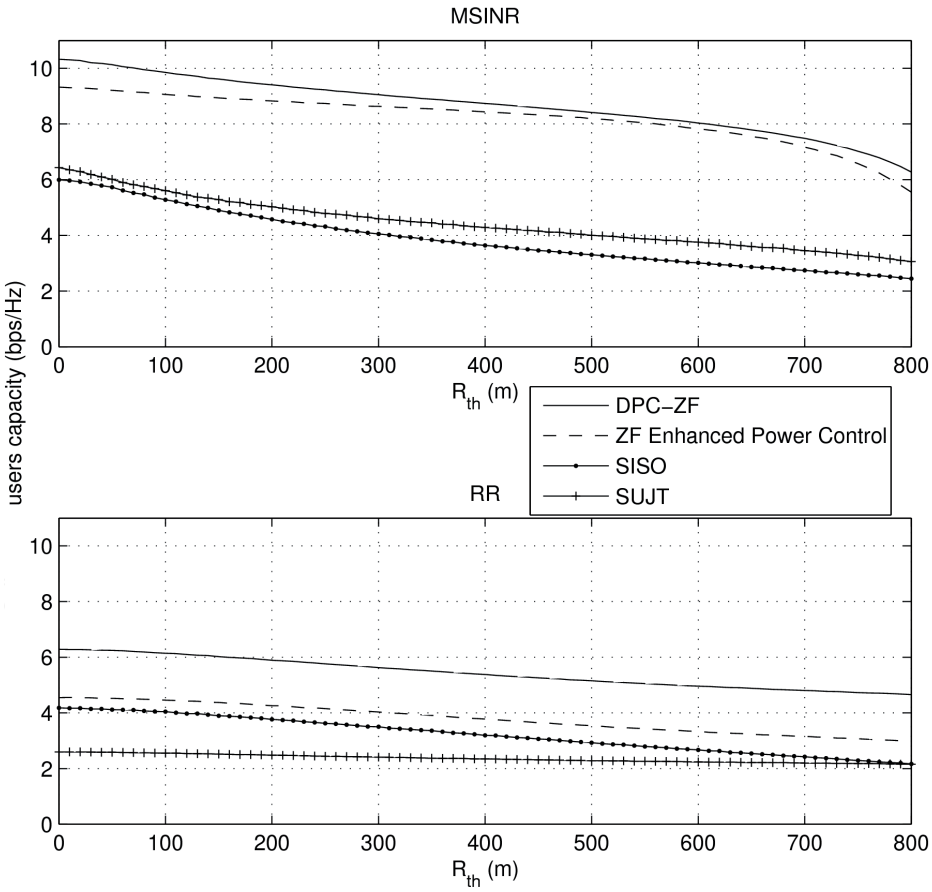

FIGURE 2.4: Cell-edge users capacity.

to their proximity to the serving BS. Focusing on the cell-edge performance, SU-JT remarkably outperforms the rest of techniques in terms of SINR but it is worth stressing the single-user character of this solution. ZF-DPC provides an advantage over ZF that is most significant when using RR scheduling. Results for non-FFR systems are greatly influenced by the scheduling policy. While for the RR scheduler provides rather low SINR values, for both 1-sector and 3-sector architectures, the MSINR scheduler delivers high SINRs, specially for non-sectorized architectures. This is because in this latter case, only close-to-BS users are being served. In contrast, it is noticeable that for FFR-based schemes, differences between RR and MSINR scheduling are not so pronounced. This is a direct consequence of the FFR design: by dividing the cell into center and edge areas, and allocating resources to both part, some degree of fairness is already enforced independently of the user selection policy.

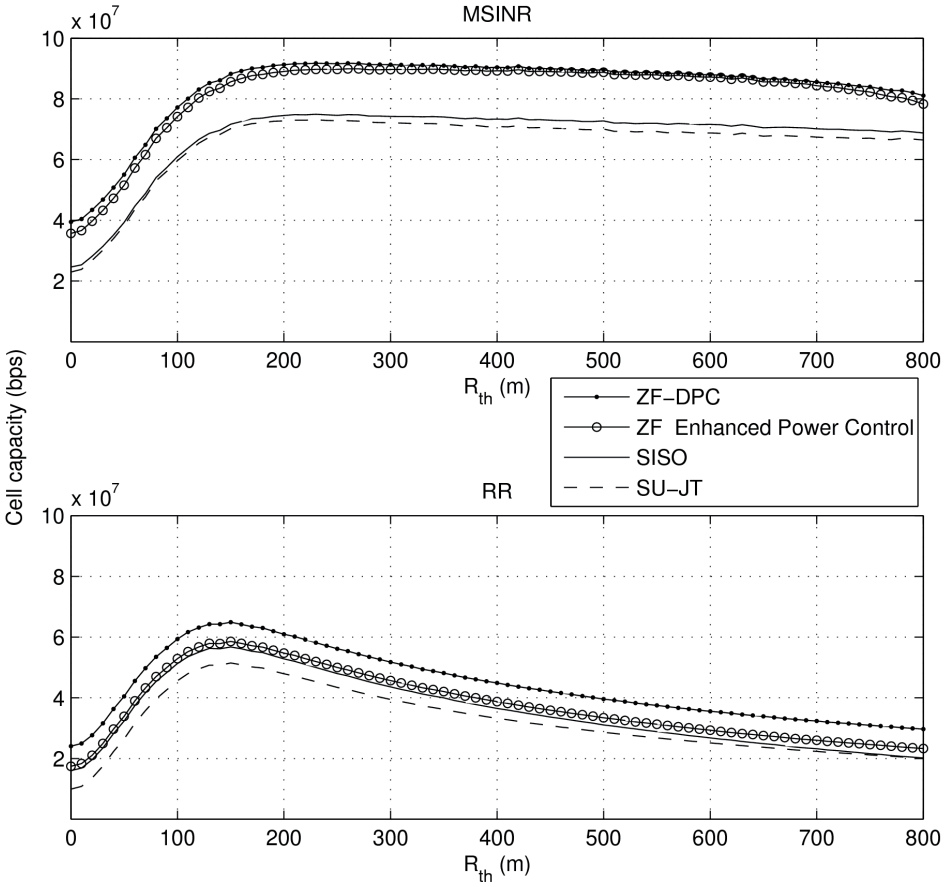

FIGURE 2.5: Overall cell capacity.

Table 2.3 presents the corresponding mean cell capacities for the different schemes. Many of the facts observed regarding SINR carry over when looking at mean cell capacity, although some remarkable differences surface. The first important fact is the confirmation that, when using a RR scheduler, FFR-based schemes provide a significant advantage in terms of capacity with respect to non-FFR architectures. In MSINR cases, non-FFR schemes provides a cell capacity higher than FFR cases in exchange for a total sacrifice of fairness. Within the non-FFR schemes, and in line with the mean SINR results, sectorization under MSINR is a critical factor to increase capacity. Focusing now on the FFR-based schemes, it can be observed how large SINRs in cell-centre users directly translates to large mean cell capacities. The same can be said for the ZF-DPC and ZF processing CoMP schemes. In contrast, note how the large SINR increase of SU-JT with respect to a 3-sector non-FFR architecture, does not translate into a larger mean cell capacity due to its single-user character. As with the SINR, it can be appreciated how

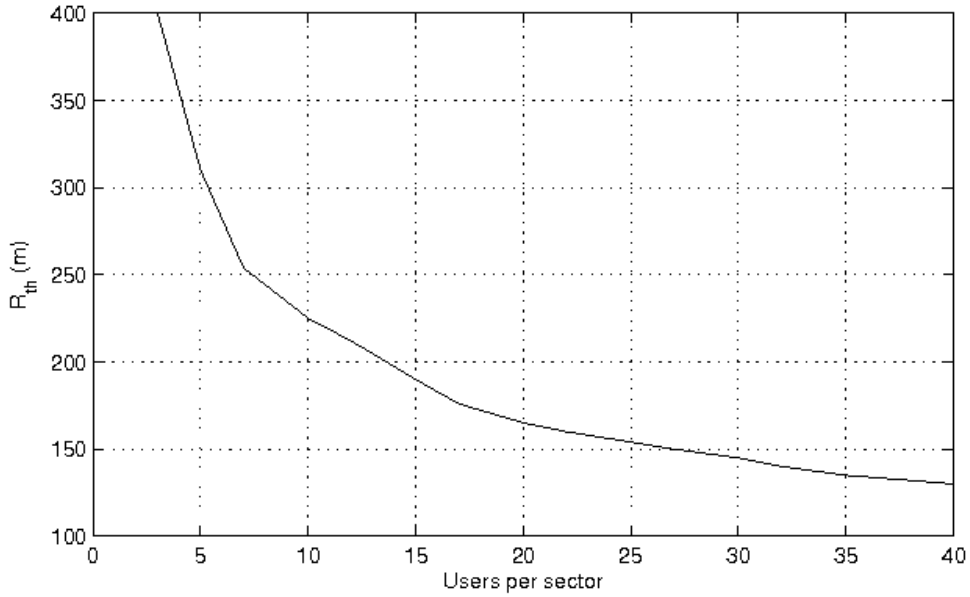

FIGURE 2.6: R_{th} optimum that maximize cell-center users capacity for RR schemes.

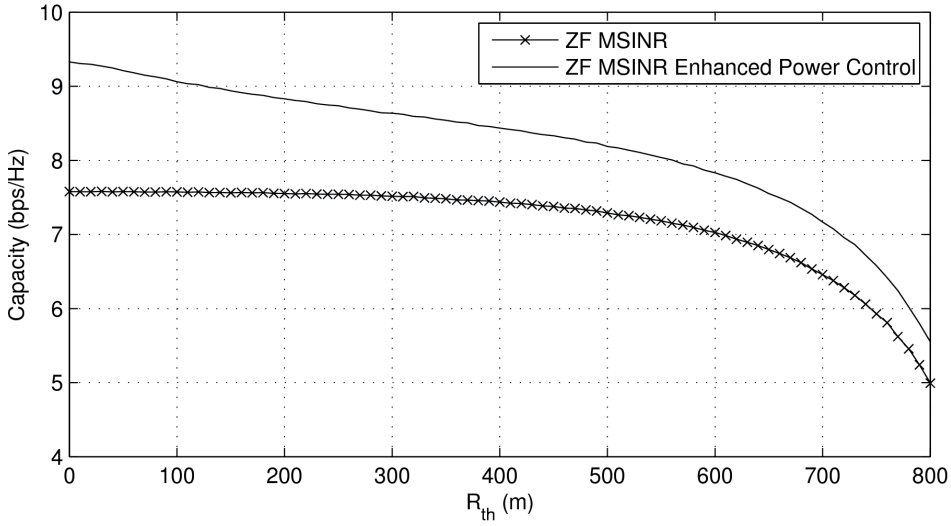

FIGURE 2.7: Enhanced power allocation ZF *vs* conventional power allocation.

MSINR scheduling leads to larger mean cell capacities than RR, with these differences being exacerbated for the cell-centre users and cell-edge users with ZF-DPC processing.

2.5.3 Complexity considerations

It is worth noting the different backhaul and complexity requirements each CoMP technique entails. Regarding backhaul capacity, ZF and ZF-DPC require of a backhaul with enough capacity to support the exchange of user data and channel state information for

all users that are being cooperatively served. In contrast, SU-JT relies on the backhaul just to share the user data. Channel information needs not be shared as the precoder design at a given BS only requires of the information between that BS and the served user. In terms of complexity, ZF and SU-JT are computationally simple as they rely on linear processing, unlike ZF-DPC where the step in going from (2.15) to (2.16) requires of complex non-linear processing to completely cancel the intra-cluster interference. In light of there remarks and the results presented so far, it seems that ZF precoding represents an attractive compromise in the capacity *vs* complexity plane.

Chapter 3

FFR design for network MIMO: Multiple antennas scenario

3.1 System model

This chapter generalizes the study presented in chapter 2 by allowing the use of multiple antennas at the transmitter and at the receiver. Furthermore, decissions regarding the operating region of a user (centre or edge) is based on the more realistic metric of received SINR, rather than distance from the BS. To this end, a downlink MU-MIMO cellular system based on OFDMA with 21 cells is considered. In this case each cell is divided into three 120^o sectors, each served by M_E sectorial antennas. The BS antennas are co-located and a uniform power P_{sc} is allocated per subcarrier. A total of N_u users, each with N_R antennas, are uniformly distributed in each sector. If the Signal to Interference plus Noise Rate (SINR) is higher than the SINR threshold γ_{th}, the user is deemed to belong to the cell-center. The rest of users are considered to belong to the cell-edge. As in the SISO case, the total bandwidth is split into two bands, B_C and B_E, allocated to cell center and cell edge areas, respectively. Furthermore, the cell edge bandwidth B_E is divided into three equal subbands, namely, B_{E_1}, B_{E_2} and B_{E_3}, that can be allocated to different sectors in two ways depending on the transmission scheme employed. Noncooperative schemes use the regular distribution (Fig. 3.2b) where all the sectors with the same main-beam direction are allocated the same frequency band. A rearranged distribution is used by CoMP schemes, where the sectors with antennas

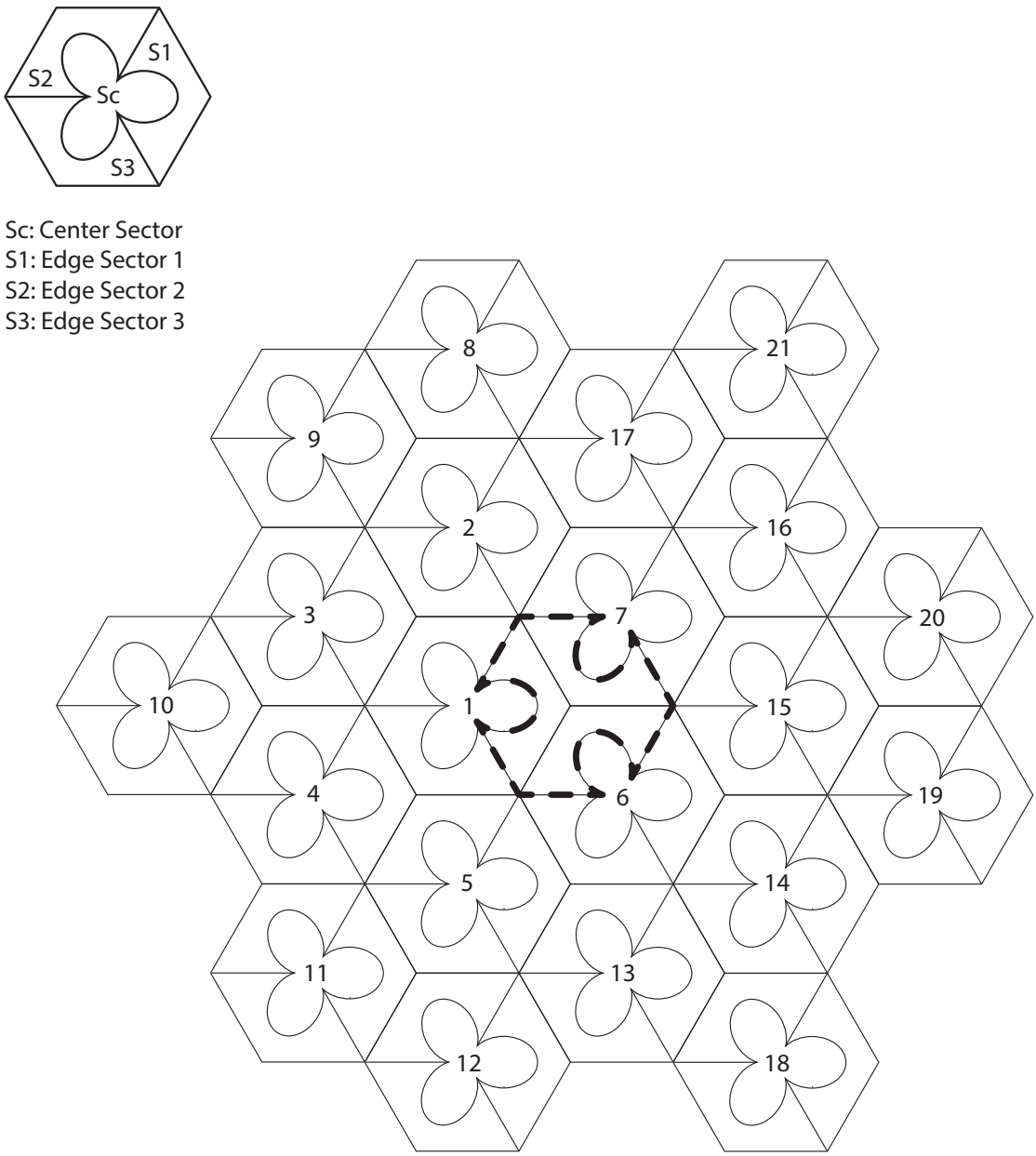

FIGURE 3.1: 21-cell Network (MIMO schemes).

pointing to the same area have the same frequency band (Fig. 3.2c). Those sectors are organized in clusters (Fig. 3.2c dotted lines). A cluster is formed by three neighbour sector BSs working in a cooperative way on the same frequency subband. Each BS has a power constraint. As in SISO, a subcarrier bandwidth equal to Δf, and a total bandwidth B is assumed. The system has $N_{SC} = B/\Delta f$ subcarriers, out of which $N_{SC}^{c} = B_C/\Delta f$ are allocated to the center region and $N_{SC}^{e} = B_{E_i}/\Delta f$ to each of the edge sectors.

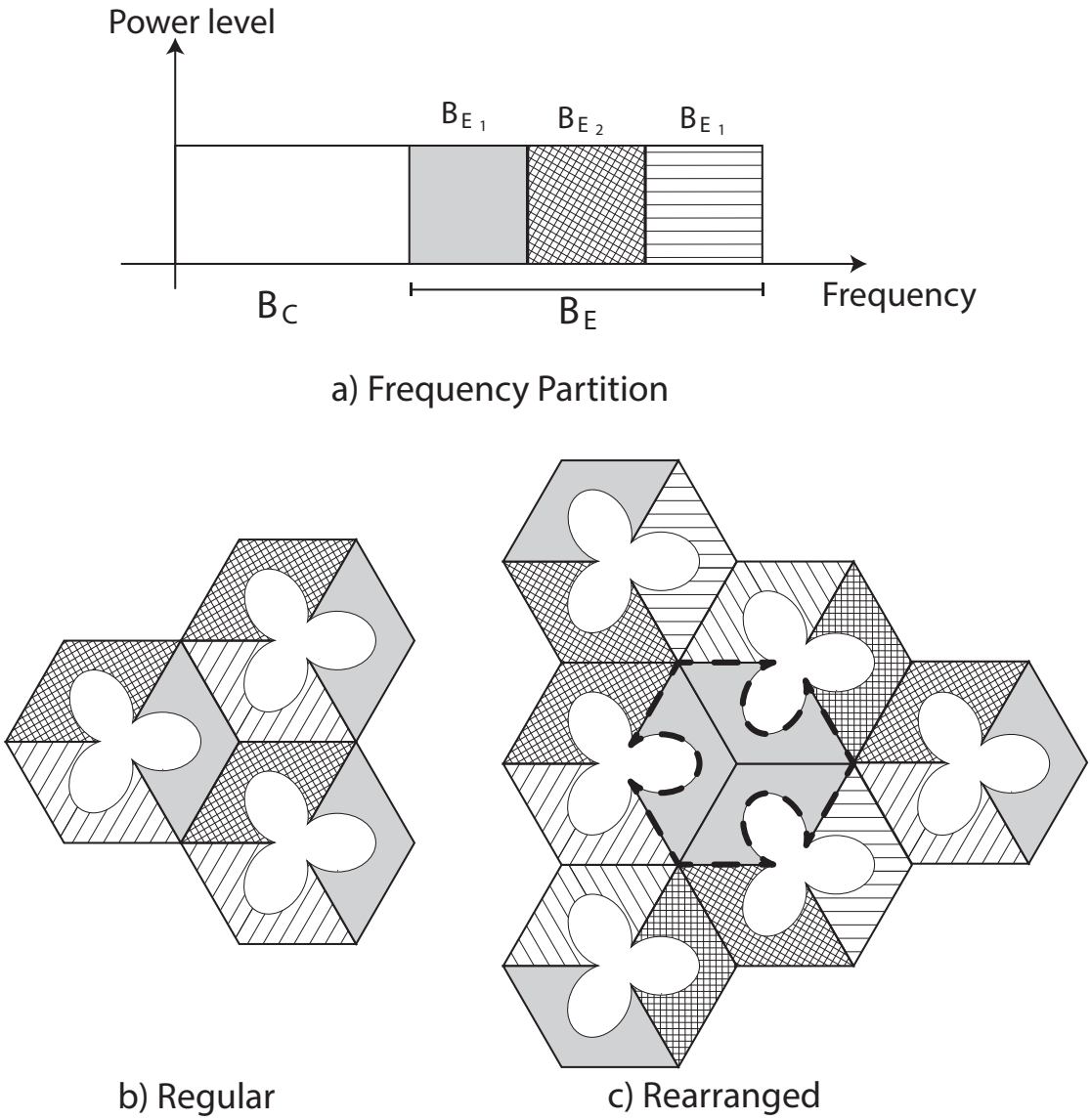

FIGURE 3.2: Frequency Partition (MIMO schemes).

The channel response linking an arbitrary antenna j from BS s and antenna i from a generic user u on an arbitrary subcarrier is modelled as described as

$$h^u_{s,i,j} = \alpha^u_{s,i,j}\sqrt{\beta^u_s A(\theta^u_{s,i,j}) PL^u_s} \tag{3.1}$$

where $\alpha^u_{s,i,j}$ and β^u_s are the fast Rayleigh fading and shadowing gains respectively; $A(\theta^u_{s,i,j})$ is the antenna gain pattern at angle $\theta^u_{s,i,j} \in [-180°, 180°]$, representing the pointing angle between antenna j from BS s and user antenna i with respect to the main-beam direction of the considered antenna; and PL^u_s is the path loss factor between

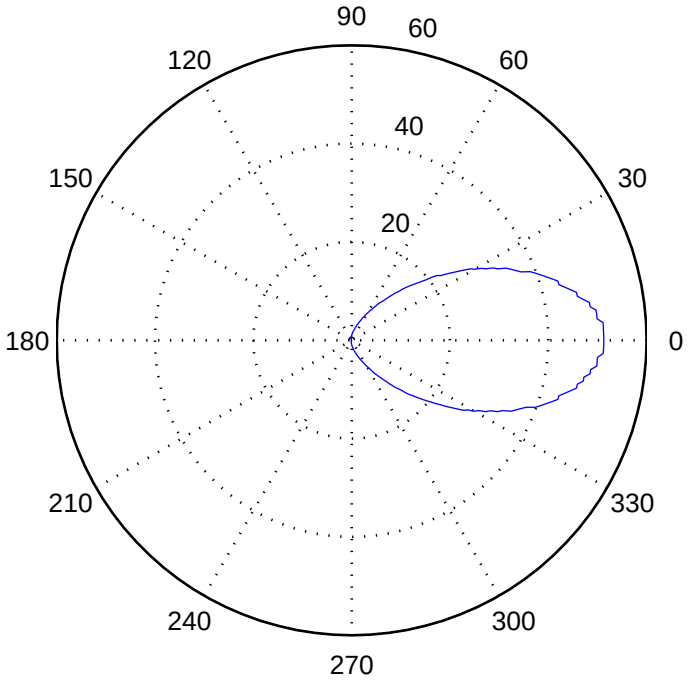

FIGURE 3.3: Horizontal radiation diagram.

user u and BS s. The path loss model used in this work is given by [12]

$$PL_s^u(dB) = -40(1 - 4 \cdot 10^{-3} \triangle h_b) \log_{10} d_{s,u} + 18 \log_{10} \triangle h_b - 21 \log_{10} f_c - 80 \quad (3.2)$$

where $d_{s,u}$ is the distance between BS s and user u, f_c is the carrier frequency in MHz and $\triangle h_b$ is the BS antenna height, measured in metres from the average roof top level. The values used in this work for these parameters are $\triangle h_b = 15$ m and $f = 2000$ MHz, leading to:

$$PL_s^u(dB) = -128.1 - 37.6 \log_{10} d_{s,u} \quad (3.3)$$

The gain pattern used for each sector antenna is computed with the measures of the horizontal radiation diagram (Fig. 3.3). This pattern corresponds to the antenna model *MP20-65* manufactured by *CSS Antenna, Inc.* for tilt and electrical tilt equal to 0.

Since shadowing is due to the influence of local topographic features and man-made structures, it is reasonable to think that there must be certain correlation between shadowing coefficients from different base stations at the same location. The two dimensional

model with spatial and BS correlation described in [13] was chosen for the computation of the shadowing factor β_s^u.

3.2 PHY-layer characterization

3.2.1 Cell-center users

To eliminate intra-cell interference within the cell center, the BS uses Block Diagonalization (BD). Given an arbitrary cell s, let us denote by $\mathbf{H}_{s,u} \in \mathbb{C}^{N_R \times M_c}$ the channel matrix linking the cell centre transmit antenna array with the cell center user u, with each entry in $\mathbf{H}_{s,u}$ conforming to the propagation model given in (2.1). Note that given the subcarrier-based operation, and to simplify notation, the subcarrier index will be omitted unless otherwise stated. Furthermore it is assumed that the maximum number of streams (N_R) are allocated to each selected user. Block diagonalization allows the simultaneous communication with up to $K = \left\lfloor \frac{M_c}{N_R} \right\rfloor$ users, where $\lfloor \, . \, \rfloor$ denotes the floor operator. To this end, let $\mathcal{U}_s$ denote the subset of selected users with $|\mathcal{U}_s| \leq K$ users. Given the linear nature of BD the transmitted symbol vector for a specific user u can be expressed as

$$\mathbf{x}_{s,u} = \mathbf{W}_{s,u}\mathbf{s}_{s,u} \ ,$$

with $\mathbf{W}_{s,u} \in \mathbb{C}^{M_c \times N_R}$ and $\mathbf{s}_{s,u} \in \mathbb{C}^{N_R \times 1}$ representing the precoding matrix and the information symbols for the selected user u, respectively. The overall precoding equation for all selected users can then be expressed as

$$\mathbf{x}_s = \mathbf{W}_s\mathbf{s}_s,$$

where $\mathbf{W}_s = \left[\mathbf{W}_{s,1} \, \mathbf{W}_{s,2} \ldots \mathbf{W}_{s,|\mathcal{U}_s|}\right] \in \mathbb{C}^{M_c \times |\mathcal{U}_s| N_R}$ and $\mathbf{s}_s = \left[\mathbf{s}_{s,1}^T \, \mathbf{s}_{s,2}^T \ldots \mathbf{s}_{s,|\mathcal{U}_s|}^T\right]^T \in \mathbb{C}^{|\mathcal{U}_s| N_R \times 1}$. The received signal for the selected user u in cell-center area of cell 1 (central cell) can be computed as

$$\mathbf{y}_{1,u} = \mathbf{H}_{1,u}\mathbf{x}_1 + \sum_{\substack{s>1 \\ s \in \mathcal{B}s}} \mathbf{H}_{s,u}\mathbf{x}_s + \boldsymbol{\eta}_{1,u} \ , \tag{3.4}$$

with $\boldsymbol{\eta}_{1,u} \in \mathbb{C}^{N_R \times 1}$ being a sample vector of a circularly symmetric zero-mean additive white Gaussian noise and $\mathcal{B}s$ the set of cells in the system.

Multi-user intra-cell interference is cancelled because BD transmission imposes the constraint $\mathbf{H}_{s,u'}\mathbf{W}_{s,u} = 0$ for $u \neq u'$. This forces $\mathbf{W}_{s,u}$ to lie in the null space of $\tilde{\mathbf{H}}_{s,u} = [\mathbf{H}_{s,1}^T \dots \mathbf{H}_{s,u-1}^T \ \mathbf{H}_{s,u+1}^T \dots \mathbf{H}_{s,|\mathcal{U}_s|}^T]^T$ assuming the dimension of this null space is greater than 0 for all users (satisfied when $\text{rank}(\tilde{\mathbf{H}}_{s,u}) < M_C$) to enable transmission. Let us define the singular value decomposition (SVD) of $\tilde{\mathbf{H}}_{s,u}$ as

$$\tilde{\mathbf{H}}_{s,u} = \tilde{\mathbf{U}}_{s,u}\tilde{\mathbf{\Sigma}}_{s,u}\left[\tilde{\mathbf{V}}_{s,u}^{(1)} \quad \tilde{\mathbf{V}}_{s,u}^{(0)}\right]^H, \tag{3.5}$$

where $\tilde{\mathbf{V}}_{s,u}^{(1)}$ contains the first $\tilde{r}_{s,u} = \text{rank}(\tilde{\mathbf{H}}_{s,u})$ right singular vectors of $\tilde{\mathbf{H}}_{s,u}$. Consequently, $\tilde{\mathbf{V}}_{s,u}^{(0)}$ forms an orthogonal basis for the null space of $\tilde{\mathbf{H}}_{s,u}$ with $\text{rank}(\tilde{\mathbf{V}}_{s,u}^{(0)}) = M_C - \tilde{r}_{s,u}$ and its columns (or their linear combinations) define the precoder matrix $\mathbf{W}_{s,u}$. It is safely assumed that N_R rows of $\mathbf{H}_{s,u}$ are necessarily linearly independent of the rows of $\tilde{\mathbf{H}}_{s,u}$ to satisfy that the number of streams transmitted to user u to be equal to $N_R = \bar{r}_{s,u} = \text{rank}(\mathbf{H}_{s,u}\tilde{\mathbf{V}}_{s,u}^{(0)})$. The new equivalent channel matrix without intra-cell interference can then be written as

$$\mathbf{H}'_{s,u} = \mathbf{H}_{s,u}\tilde{\mathbf{V}}_{s,u}^{(0)}.$$

As noted in [5], the sum-rate optimization of the transmit and receive filters (i.e., precoder and equalizer) requires in general of an iterative procedure. As in [5], a more practical approach, and the one followed in this work, is to base the design on the SVD of the equivalent channel matrix,

$$\mathbf{H'}_{s,u} = \ \mathbf{U}_{s,u}\begin{bmatrix} \mathbf{\Sigma}_{s,u} & 0 \\ 0 & 0 \end{bmatrix}\left[\mathbf{V}_{s,u}^{(1)} \quad \mathbf{V}_{s,u}^{(0)}\right]^H, \tag{3.6}$$

where $\mathbf{\Sigma}_{s,u}$ is a diagonal matrix containing the singular values of the equivalent channel matrix, that is,

$$\mathbf{\Sigma}_{s,u} = \mathcal{D}\left([\sigma_{s,u}^1 \ \dots \ \sigma_{s,u}^{N_R}]\right).$$

The precoder matrix is then given by

$$\mathbf{W}_s = \left[\ \tilde{\mathbf{V}}_{s,1}^{(0)}\mathbf{V}_{s,1}^{(1)} \quad \dots \quad \tilde{\mathbf{V}}_{s,|\mathcal{U}_s|}^{(0)}\mathbf{V}_{s,|\mathcal{U}_s|}^{(1)}\ \right]\mathbf{\Lambda}_s^{1/2} \tag{3.7}$$

where

$$\mathbf{\Lambda}_s = \mathcal{D}\left(\left[\mathbf{\Lambda}_{s,1} \ \dots \ \mathbf{\Lambda}_{s,|\mathcal{U}_s|}\right]\right)$$

and

$$\mathbf{\Lambda}_{s,u} = \mathcal{D}\left([\lambda_{s,u}^1 \ \dots \ \lambda_{s,u}^{N_R}]\right),$$

is a diagonal power allocation matrix whose elements are computed by applying the waterfilling algorithm on the diagonal matrix defined by

$$\mathbf{\Sigma}_s = \mathcal{D}\left(\left[\mathbf{\Sigma}_{s,1} \ \dots \ \mathbf{\Sigma}_{s,|\mathcal{U}_s|}\right]\right), \tag{3.8}$$

while assuming a total power constraint per subcarrier of P_{sc}. Considering now that each user u uses the decoder unitary matrix $\mathbf{D}_{s,u} = \mathbf{U}_{s,u}^H$, the estimated symbol vector of user u in cell 1 can be expressed as

$$\begin{aligned}\hat{\mathbf{s}}_{1,u} = &\underbrace{\mathbf{\Sigma}_{1,u}\mathbf{\Lambda}_{1,u}^{1/2}\mathbf{s}_{1,u}}_{\text{desired signal}} + \underbrace{\mathbf{U}_{1,u}^H \sum_{\substack{s>1 \\ s\in\mathcal{B}s}} \mathbf{H}_{s,u}\mathbf{W}_s\mathbf{s}_s}_{\text{inter-cell interference}} \\ &+ \underbrace{\mathbf{U}_{1,u}^H\boldsymbol{\eta}_{1,u}}_{\text{noise}}.\end{aligned} \tag{3.9}$$

Finally, the SINR experienced by stream i of cell-center user u connected to BS s is found to be

$$\gamma_{s,u}^{i\ \mathrm{c}} = \frac{(\sigma_{s,u}^i)^2|\lambda_{s,u}^i|}{\sigma_\eta^2 + \sum_{s'\neq s}\sum_{j=1}^{M_C}\sum_{z=1}^{N_R}|h_{s,u}^{z,j}w_{s'}^{z,j}|^2}. \tag{3.10}$$

In this way, the instantaneous capacity achieved by cell-center user u (on a given subcarrier) can be written as

$$C_u^{\mathrm{c}} = \Delta f \sum_{i=1}^{\bar{r}_{s,u}} \log_2(1+\gamma_{s,u}^{i\ \mathrm{c}}). \tag{3.11}$$

3.2.2 Cell-edge users

As in the SISO case, cell-edge users can be cooperatively served by three neighbouring BS sectors conforming a cluster or can be non-cooperatively served by each BS sector individually (Frequency Reuse 3 scheme). Cooperation can be implemented by means of

different algorithms. In this work different techniques are considered, namely, ZF-BD, ZF-DPC, SU-JT, JT-ZF, ZF-BD-suboptim, ZF-DPC-suboptim and SU-JT-suboptim.

3.2.2.1 Zero Forcing - Block Diagonalization (ZF-BD)

In this case, the transmission scheme is very similar to that used to serve the cell-center users. Unfortunately, the design is complicated by the fact that now per-BS power constraints must be taken into account. Let us denote by $\mathcal{C}$ the set of clusters, such as the one shown in figure 3.2, transmitting on subcarrier n. Sector BSs $\mathcal{B}_c$ in cluster c cooperate to transmit to a set of users $\mathcal{U}_c$ in the sectors they cover. The channel linking the coordinated transmit antenna arrays with an arbitrary user u in the cell edge is denoted by the $N_R \times N_T$ matrix $\mathbf{H}_{c,u}$ where $N_T = |\mathcal{B}_c| M_E$. The transmit signal vector from the BS $b \in \mathcal{B}_c$ is given by

$$\mathbf{x}_{c,b} = \tilde{\mathbf{W}}_{c,b} \mathbf{s}_c$$

where $\tilde{\mathbf{W}}_{c,b} \in \mathbb{C}^{M_E \times |\mathcal{U}_c| N_R}$ is the precoding matrix and $\mathbf{s}_c \in \mathbb{C}^{|\mathcal{U}_c| N_R \times 1}$ is the vector containing all symbols to be transmitted to the selected user group.

The overall precoding matrix encompassing the $|\mathcal{B}_c|$ sectors is then given by

$$\mathbf{W}_c = [\tilde{\mathbf{W}}_{c,1}^T \ \dots \ \tilde{\mathbf{W}}_{c,|\mathcal{B}_c|}^T]^T,$$

allowing a compact representation of the reception equation as

$$\mathbf{y}_u = \mathbf{H}_{c,u} \mathbf{W}_c \mathbf{s}_c + \sum_{\substack{c' \neq c \\ c' \in \mathcal{C}}} \mathbf{H}_{c',u} \mathbf{W}_{c'} \mathbf{s}_{c'} + \boldsymbol{\eta}_u \tag{3.12}$$

Note that in order to fulfill the per-BS power constraint, it should hold that

$$\mathrm{Tr}(\tilde{\mathbf{W}}_{c,b} \tilde{\mathbf{W}}_{c,b}^H) < P_{sc}, \quad \forall b \in \{1 \dots |\mathcal{B}_c|\}. \tag{3.13}$$

For convenience, the precoding matrix can also be defined from the point of view of the received antennas as

$$\mathbf{W}_c = [\mathbf{W}_{c,1} \ \dots \ \mathbf{W}_{c,|\mathcal{U}_c|}],$$

with $\mathbf{W}_{c,k} \in \mathbb{C}^{N_T \times N_R}$. In this case (3.13) can be rewritten as

$$\sum_{u=1}^{|\mathcal{U}_c|} \mathrm{Tr}(\mathbf{B}_b \mathbf{W}_{c,u} \mathbf{W}_{c,u}^H) < P_{sc}, \quad \forall b \in \{1 \dots |\mathcal{B}_c|\} \tag{3.14}$$

where

$$\mathbf{B}_b \triangleq \mathcal{D}\left(\underbrace{0,\dots,0,}_{(b-1)M_E}\underbrace{1,\dots,1,}_{M_E}\underbrace{0,\dots,0,}_{(|\mathcal{B}_c|-b)M_E}\right).$$

Following the re-arranged frequency partition introduced in [8] and illustrated in figure 3.2, it is easy to observe that the closest interfering BS with a directional antenna pattern pointing towards cluster c is at a distance $2R + L$, where L denotes the (hexagonal) cell apothem and R the (circular) cell radius. Despite the envisaged low power of the intercell interference, in this work, and in order to further improve the performance of the system, the interference is modeled as Gaussian noise (e.g. Gaussian hypothesis) when designing the optimal filters. To this end, each entry $\tilde{y}_u$ in the the interference plus noise vector given by

$$\tilde{\mathbf{y}}_\mathbf{u} = \sum_{\substack{c' \neq c \\ c' \in \mathcal{C}}} \mathbf{H}_{c',u} \mathbf{W}_{c'} \mathbf{s}_{c'} + \boldsymbol{\eta}_u,$$

is assumed to be independent and Gaussian distributed, that is, $\tilde{y}_u \backsim \mathcal{N}(0, \sigma^2_{\tilde{y}_u})$ and $E\{\tilde{\mathbf{y}}_\mathbf{u}\tilde{\mathbf{y}}_\mathbf{u}^\mathbf{H}\} = \sigma^2_{\tilde{y}_u}\mathbf{I}$. Then, the sum-rate maximization problem becomes [14],

$$\begin{aligned} \max_{\mathbf{S}_{c,1}\ ,\ \dots\ ,\mathbf{S}_{c,|\mathcal{U}_c|}} \quad & \sum_{u=1}^{|\mathcal{U}_c|} \log_2 \left| \mathbf{I} + \frac{1}{\sigma^2_{\tilde{y}_u}} \mathbf{H}_{c,u} \mathbf{S}_{c,u} \mathbf{H}_{c,u}^H \right| \\ \text{subject to} \quad & \mathbf{H}_{c,u'} \mathbf{W}_{c,u} = 0, \ \forall u \neq u', \\ & \sum_{u=1}^{|\mathcal{U}_c|} \mathrm{Tr}(\mathbf{B}_b \mathbf{S}_{c,u}) < P_{sc}, \forall b \in \{1 \dots |\mathcal{B}_c|\} \\ & \mathbf{S}_{c,u} \succeq \mathbf{0}, \ \forall u. \end{aligned} \tag{3.15}$$

where $\mathbf{S}_{c,u} = \mathbf{W}_{c,u}\mathbf{W}_{c,u}^H$.

Extending the definition of $\tilde{\mathbf{H}}_{c,u}$ to the cell edge users, and in order to eliminate all intra cluster interference by means of BD, the precoder must include the columns of $\tilde{\mathbf{V}}_{c,u}^{(0)}$ defined as in (3.5). Moreover, as proved in [14], the precoding covariance matrix takes the form

$$\mathbf{S}_{c,u} = \tilde{\mathbf{V}}_{c,u}^{(0)} \mathbf{Q}_{c,u} \tilde{\mathbf{V}}_{c,u}^{(0)H}.$$

Thus, the convex optimization problem can be rewritten as

$$\begin{aligned} &\max_{\mathbf{Q}_{c,1}\ ,\ \cdots\ ,\mathbf{Q}_{c,|\mathcal{U}_c|}} \sum_{u=1}^{|\mathcal{U}_c|} \log_2 \left| \mathbf{I} + \tfrac{1}{\sigma^2_{\tilde{y}_u}} \mathbf{H}_{c,u} \tilde{\mathbf{V}}^{(0)}_{c,u} \mathbf{Q}_{c,u} \tilde{\mathbf{V}}^{(0)H}_{c,u} \mathbf{H}^H_{c,u} \right| \\ &\text{subject to} \\ &\quad \sum_{u=1}^{|\mathcal{U}_c|} \mathrm{Tr}(\mathbf{B}_b \tilde{\mathbf{V}}^{(0)}_{c,u} \mathbf{Q}_{c,u} \tilde{\mathbf{V}}^{(0)H}_{c,u}) < P_{sc}, \forall b \in \{1 \dots |\mathcal{B}_c|\} \\ &\quad \mathbf{Q}_{c,u} \succeq \mathbf{0},\ \forall u. \end{aligned} \tag{3.16}$$

The problem is solved by combining Lagrange duality optimization and the ellipsoid method [15]. To this end, let us define matrix $\mathbf{\Psi}_{c,u} \triangleq \mathbf{H}_{c,u} \tilde{\mathbf{V}}^{(0)}_{c,u} \left((\tilde{\mathbf{V}}^{(0)}_{c,u})^H \mathbf{B}_\lambda \tilde{\mathbf{V}}^{(0)}_{c,u} \right)^{-1/2}$ and its associated SVD decomposition,

$$\mathbf{\Psi}_{c,u} = \hat{\mathbf{U}}_{c,u} \hat{\mathbf{\Sigma}}_{c,u} \hat{\mathbf{V}}^H_{c,u}. \tag{3.17}$$

Now, using results from [14], it can be shown that the estimate symbol vector of user u is similar to expression (3.9) and given by

$$\begin{aligned} \hat{\mathbf{s}}_{c,u} = \underbrace{\hat{\mathbf{\Sigma}}_{c,u} \hat{\mathbf{\Lambda}}^{1/2}_{c,u} \mathbf{s}_{c,u}}_{\text{desired signal}} + \underbrace{\hat{\mathbf{U}}^H_{c,u} \sum_{\substack{c' \neq c \\ c' \in \mathcal{C}[n]}} \mathbf{H}_{c,u} \mathbf{W}_{c'} \mathbf{s}_{c'}}_{\text{inter-cluster interference}} \\ + \underbrace{\hat{\mathbf{U}}^H_{c,u} \boldsymbol{\eta}_{c,u}}_{\text{noise}}. \end{aligned} \tag{3.18}$$

where $\hat{\mathbf{\Lambda}}_{c,u}$ is a diagonal power allocation matrix whose elements are computed by applying waterfilling on the diagonal matrix $\hat{\mathbf{\Sigma}}_{c,u}$ while assuming a total power constraint of P_{sc}. The diagonal matrix $\mathbf{B}_\lambda$ contains the values of the Lagrange multipliers used to iteratively solve the convex optimization problem. Further details leading to the solution of (3.16) can be found in [14].

Using the precoder solution to (3.16), the SINR experienced by stream i of cell-edge user u connected to cluster c when using ZF-BD is found to be

$$\gamma^{i\ \ ZF-BD}_{c,u} = \frac{(\hat{\sigma}^i_{c,u})^2 \hat{\lambda}^i_{c,u}}{\sigma^2_\eta + \sum_{c' \neq c} \sum_{j=1}^{n_T} \sum_{z=1}^{N_R} |h^{z,j}_{c,u} w^{z,j}_{c'}|^2}, \tag{3.19}$$

and the instantaneous capacity allocated to cell-center user u on an arbitrary subcarrier can then be written as

$$C_u = \Delta f \sum_{i=1}^{\bar{r}_{c,u}} \log_2(1 + \gamma_{c,u}^{i\ ZF-BD}), \tag{3.20}$$

3.2.2.2 ZF-DPC - Block Diagonalization (ZF-DPC-BD)

Given a fixed encoding order for the transmitted signals to different MSs, only causal interference among symbols transmitted to MSs being cooperatively served need to be cancelled. The non-causal interference can be eliminated by using successive interference cancellation (SIC) at the receiver side or by using DPC at the transmitter side. Assuming the use of DPC at the transmitter side, it is possible to modify (3.15) to pose the maximization problem suitably adapted to ZF-DPC precoding [7] by substituting the BD constraints

$$\mathbf{H}_{c,u'}\mathbf{W}_{c,u} = 0,\ \forall u \neq u',$$

by the DPC constraints

$$\mathbf{H}_{c,u'}\mathbf{W}_{c,u} = 0,\ \forall u > u'.$$

The resulting problem can be similarly solved in (3.15) by simply changing the definition of $\tilde{\mathbf{H}}_{s,u} = [\mathbf{H}_{s,1}^T \dots \mathbf{H}_{s,u-1}^T\ \mathbf{H}_{s,u+1}^T \dots \mathbf{H}_{s,|\mathcal{U}_s|}^T]^T$ by $\tilde{\mathbf{H}}_{s,u} = [\mathbf{H}_{s,u+1}^T \dots \mathbf{H}_{s,|\mathcal{U}_s|}^T]^T$, $\forall u \in \{1 \dots |\mathcal{U}_s| - 1\}$, that is, retaining only the causal interference terms. Note that for user $u = |\mathcal{U}_s|$, no constraints need to be enforced, thus $\tilde{\mathbf{V}}_{s,u}^{(0)} = \mathbf{I}_{N_T}$.

3.2.2.3 Single user-Joint transmission (SU-JT)

For comparison purposes, we also consider the use of SU-JT where the set of sector BSs in each cluster cooperate to transmit to a single user. Consequently, there is not intra-cluster interference and the maximization problem (3.15) is only subject to the per-base power constraints. The problem is solved analogously with the difference that the computation of $\tilde{\mathbf{V}}_{s,u}^{(0)}$ can be skipped (i.e., $\tilde{\mathbf{V}}_{s,u}^{(0)} = \mathbf{I}_{N_T}\ \ \forall u$).

3.2.2.4 Joint Transmission Zero Forcing (JT-ZF)

Joint transmitter zero forcing approach can be viewed as the MIMO versions of the technique presented in Section 2.2.2.3 (page 10). Defining the cluster c cooperative channel matrix as $\mathbf{H}_c = [\mathbf{H}_{c,1}^T \dots \mathbf{H}_{c,|\mathcal{U}_c|}^T]^T$, the precoding matrix takes the form

$$\mathbf{W}_c = \mathbf{H}_c^H (\mathbf{H}_c \mathbf{H}_c^H)^{-1} \mathbf{G}_c = \mathbf{W}'_c \mathbf{G}_c \tag{3.21}$$

where $\mathbf{G}_c$ is a diagonal power allocation matrix

$$\mathbf{G}_c = \mathcal{D}(g_{(1,1)}, \dots, g_{(\bar{r}_{c,1},1)} \dots g_{(1,|\mathcal{U}_c|)}, \dots, g_{(\bar{r}_{c,|\mathcal{U}_c|},|\mathcal{U}_c|)}) \in \mathbb{C}^{|\mathcal{U}_c|N_R \times |\mathcal{U}_c|N_R} \tag{3.22}$$

that guarantees the per-BS power constraints with $g_{i,u}$ representing the allocated power for the corresponding original data stream i of user u (note that the number of streams transmitted to user u is equal to $N_R = \bar{r}_{c,u}$). Since typically $|\mathcal{U}_c|N_R = N_{R_{tot}} \gg |\mathcal{B}_c|$ and there are only $|\mathcal{B}_c|$ per-BS power constraints in (3.13), we can further divide the set of elements $g_{i,u}$ into $|\mathcal{B}_c|$ groups, each with $N_{R_{tot}}/|\mathcal{B}_c|$ elements having the same value:

$$\mathbf{G}_c = \mathcal{D}(g_1 \mathbf{I}_{(N_{R_{tot}}/|\mathcal{B}_c|)}, g_2 \mathbf{I}_{(N_{R_{tot}}/|\mathcal{B}_c|)}, \dots, g_{|\mathcal{B}_c|} \mathbf{I}_{(N_{R_{tot}}/|\mathcal{B}_c|)}). \tag{3.23}$$

Defining now

$$\mathbf{Q}_{|\mathcal{B}_c|\times|\mathcal{B}_c|} = \begin{bmatrix} ||\mathbf{W'}_c^{[1,1]}||_F^2 & ||\mathbf{W'}_c^{[1,2]}||_F^2 & \cdots & ||\mathbf{W'}_c^{[1,|\mathcal{B}_c|]}||_F^2 \\ ||\mathbf{W'}_c^{[2,1]}||_F^2 & ||\mathbf{W'}_c^{[2,2]}||_F^2 & \cdots & ||\mathbf{W'}_c^{[2,|\mathcal{B}_c|]}||_F^2 \\ \vdots & \vdots & \vdots & \vdots \\ ||\mathbf{W'}_c^{[|\mathcal{B}_c|,1]}||_F^2 & ||\mathbf{W'}_c^{[|\mathcal{B}_c|,2]}||_F^2 & \cdots & ||\mathbf{W'}_c^{[|\mathcal{B}_c|,|\mathcal{B}_c|]}||_F^2 \end{bmatrix}, \tag{3.24}$$

where $||\mathbf{W'}_c^{[j,b]}||_F^2$ is an $M_E \times N_{R_{tot}}/|\mathcal{B}_c|$ submatrix in $\mathbf{W'}_c$, corresponding to the transmit weights for the sector BS b for the jth group of data streams as defined above. Defining $\mathbf{p} = [P_{sc}, \cdots, P_{sc}]_{|\mathcal{B}_c|\times 1}^T$ as the per-BS power constraint vector, $\mathbf{G}_c$ can be computed solving the linear system equation

$$\mathbf{g} = [g_1^2, g_2^2, \cdots, g_{|\mathcal{B}_c|}^2]^T = \mathbf{Q}^{-1}\mathbf{p}. \tag{3.25}$$

When the solution is unfeasible (some entries of $\mathbf{p}$ are not positive) or the system does not have a solution, $\mathbf{G}_c$ takes the form

$$\mathbf{G}_c = g\mathbf{I}, \qquad g = \min_{b=1,\cdots,|\mathcal{B}_c|} \left(\frac{P_{sc}}{||\mathbf{W'}_c^{[b]}||_F^2} \right), \tag{3.26}$$

where $\mathbf{W'}_c^{[b]}$ contains the rows of $\mathbf{W'}_c$ corresponding to transmit antennas at sector BS b. Note that while (3.25) can transmit with full power at each sector BS, when using (3.26) only one sector BS utilizes the full power. From this point onwards, this algorithm to compute the diagonal power allocation matrix fulfilling per-BS power constraints will be refered to as suboptimal power algorithm [16].

Since it holds that $\mathbf{H}_c\mathbf{W}_c = \mathbf{G}_c$, then the SINR experienced by stream i of cell-edge user u connected to cluster c when using JT-ZF is found to be

$$\gamma_{c,u}^{i\ JT-ZF} = \frac{|g_{i,u}|^2}{\sigma_\eta^2 + \sum\limits_{c' \neq c} \sum\limits_{j=1}^{n_T} \sum\limits_{z=1}^{N_R} |h_{c,u}^{z,j} w_{c'}^{z,j}|^2}, \tag{3.27}$$

and the instantaneous capacity allocated to cell-center user u on an arbitrary subcarrier can then be written as

$$C_u = \Delta f \sum_{i=1}^{\bar{r}_{c,u}} \log_2(1 + \gamma_{c,u}^{i\ JT-ZF}), \tag{3.28}$$

3.2.2.5 Zero Forcing - Block Diagonalization - Suboptimal (ZF-BD-suboptimal)

This technique is similar to ZF-BD transmission but does not solve the maximization problem. The precoding matrix can be written as

$$\mathbf{W}_c = \mathbf{W}'_c\mathbf{G}_c = [\mathbf{W}'_{c,1} \ \cdots \ \mathbf{W}_{c,|\mathcal{U}'_c|}]\mathbf{G}_c, \tag{3.29}$$

where

$$\mathbf{W}'_{c,u} = \tilde{\mathbf{V}}_{c,u}^{(0)}\hat{\mathbf{V}}'_{c,u}. \tag{3.30}$$

The precoder $\tilde{\mathbf{V}}_{c,u}^{(0)}$ eliminates all intra cluster interference and was already defined in (3.5). $\hat{\mathbf{V}}'_{c,u}$ is computed by performing the SVD of the equivalent channel matrix, $\mathbf{H}'_{c,u} = \mathbf{H}_{c,u}\tilde{\mathbf{V}}_{c,u}^{(0)} = \hat{\mathbf{U}}'_{c,u}\hat{\mathbf{\Sigma}}'_{c,u}\hat{\mathbf{V}}'^H_{c,u}$. The decoder matrix for user u is $\hat{\mathbf{U}}'^H_{c,u}$ and $\mathbf{G}_c$ is the diagonal power allocation matrix computed using the suboptimal power algorithm. Then the

estimate symbol vector of user u in cluster c can be expressed as

$$\hat{\mathbf{s}}_{c,u} = \underbrace{\hat{\mathbf{\Sigma}}'_{c,u} g_u \mathbf{I} \mathbf{s}_{c,u}}_{\text{desired signal}} + \underbrace{\hat{\mathbf{U}}'^{H}_{c,u} \sum_{\substack{c' \neq c \\ c' \in \mathcal{C}[n]}} \mathbf{H}_{c,u} \mathbf{W}_{c'} \mathbf{s}_{c'}}_{\text{inter-cluster interference}} + \underbrace{\hat{\mathbf{U}}'^{H}_{c,u} \boldsymbol{\eta}_{c,u}}_{\text{noise}}. \tag{3.31}$$

The SINR experienced by stream i of cell-edge user u connected to cluster c when using ZF-BD-suboptim is found to be

$$\gamma^{i}_{c,u}{}^{ZF-BD-subopt} = \frac{(\hat{\sigma}'^{i}_{c,u})^2 g_u^2}{\sigma_\eta^2 + \sum_{c' \neq c} \sum_{j=1}^{n_T} \sum_{z=1}^{N_R} |h^{z,j}_{c,u} w^{z,j}_{c'}|^2}, \tag{3.32}$$

and the instantaneous capacity allocated to cell-center user u on an arbitrary subcarrier can then be written as (3.28).

3.2.2.6 Zero Forcing - Dirty Paper Code - Suboptimal (ZF-BD-suboptimal)

The ZF-BD-suboptimal transmission is analogous to the one presented in Section 3.2.2.2 (page 32) but with a suboptimal power allocation strategy. The non-causal interference among symbols transmitted to MSs given a fixed encoding order for the transmitted signals to different MSs is not necessary to be cancelled. It can be eliminated by using DPC at the transmitter side. In order to eliminate causal interference among users let us define

$$\tilde{\mathbf{H}}_{s,u} = [\mathbf{H}^T_{s,u+1} \dots \mathbf{H}^T_{s,|\mathcal{U}_s|}]^T = \mathbf{U}_{s,u} \begin{bmatrix} \mathbf{\Sigma}_{s,u} & 0 \\ 0 & 0 \end{bmatrix} \begin{bmatrix} \mathbf{V}^{(1)}_{s,u} & \mathbf{V}^{(0)}_{s,u} \end{bmatrix}^H, \tag{3.33}$$

where $\tilde{\mathbf{V}}^{(0)}_{s,u}$ forms an orthogonal basis for the null space of $\tilde{\mathbf{H}}_{s,u}$ and can eliminate the causal interference. The equivalent channel matrix can then be written as $\mathbf{H}'_{c,u} = \mathbf{H}_{c,u} \tilde{\mathbf{V}}^{(0)}_{c,u} = \hat{\mathbf{U}}'_{c,u} \hat{\mathbf{\Sigma}}'_{c,u} \hat{\mathbf{V}}'^{H}_{c,u}$ and the precoding matrix is found to be like the ones shown in (3.29) and (3.30). Correspondingly, the estimate symbol vector and the SINR expresion can be written like the ones shown in (3.31) and (3.32), respectively.

3.2.2.7 Single User - Joint Transmission - Suboptim (SU-JT-subopt)

In this case all sector BSs in each cluster cooperate to transmit to a single user. There is not intra-cluster interference and the precoding matrix can be written as

$$\mathbf{W}_c = \mathbf{W}'_c \mathbf{G}_c = \mathbf{V}_{c,u} \mathbf{G}_c, \tag{3.34}$$

where $\mathbf{V}_{c,u}$ can be compute doing the SVD to channel matrix $\mathbf{H}_{c,u} = \mathbf{U}_{c,u} \mathbf{\Sigma}_{c,u} \mathbf{V}_{c,u}^H$, and $\mathbf{G}_c$ is the diagonal power allocation matrix computed with the suboptimal power algorithm. The SINR experienced by stream i of cell-edge user u connected to cluster c is found to be

$$\gamma_{c,u}^{i\ JT-ZF-subopt} = \frac{(\sigma_{c,u}^i)^2 g_u^2}{\sigma_\eta^2 + \sum\limits_{c' \neq c} \sum\limits_{j=1}^{n_T} \sum\limits_{z=1}^{N_R} |h_{c,u}^{z,j} w_{c'}^{z,j}|^2}, \tag{3.35}$$

and the instantaneous capacity has the same expression as (3.28).

3.2.2.8 Frequency Reuse 3 - noncooperative (FR3)

In this case, the system uses the Regular frequency partition shown in figure 3.2.b and each sector BS transmits to one user computing the SVD of the channel matrix and applying the waterfilling algorithm to determine the power allocation matrix as in Section 3.2.1 (page 26).

3.3 Cell-capacity

The multicarrier nature of the OFDMA system must be considered to obtain the instantaneous capacity of cell s by summing up the capacities of all the transmission channels established by the system to users in the area of cell s. The instantaneous capacity of all subcarriers allocated to cell-center users served by cell s can be written as

$$C_s^c = \Delta f \sum_{\forall u \in \mathcal{U}_s^c} \sum_{\forall n \in \mathcal{N}^c} \sum_{i=1}^{\bar{r}_{s,u}} \log_2(1 + \gamma_{s,u}^{i\ c}[n]), \tag{3.36}$$

where $\mathcal{U}_s^c$ is the set of users in the cell-center sector of cell s and $\mathcal{N}^c$ is the set of subcarriers assigned to cell-center users. The instantaneous capacity of cell-edge users

served by cell s is given by

$$C_s^E = \Delta f \sum_{\forall c \in \mathcal{D}_s} \sum_{\forall u \in \mathcal{U}_{s,c}^E} \sum_{\forall n \in \mathcal{N}_c^E} \sum_{i=1}^{\bar{r}_{c,u}} \log_2(1 + {\gamma_{c,u}^i}^E[n]), \tag{3.37}$$

where $\mathcal{D}_s$ is the set of clusters containing a sector covered by cell s, $\mathcal{U}_{s,c}^E$ is the set of users receiving data in the cell-edge sector of cell s-cluster c and $\mathcal{N}_c^E$ is the set of subcarriers allocated to cell-edge users of cluster c. Obviously, the total instantaneous capacity of cell j can be obtained as

$$C_s = C_s^c + C_s^E.$$

The ergodic (average) capacity can then be obtained by averaging (either analytically or using Monte Carlo repeated random numerical experiments) the instantaneous capacity over system parameters such as the spatial distribution of users, the fast Rayleigh fading, the shadowing, or the subcarrier allocation strategy.

3.4 User selection

In the user selection process, two scheduling strategies have been considered, namely, round robin (RR) and maximum capacity (MC). In the RR strategy, subcarriers from sets $\mathcal{N}^c$ and $\mathcal{N}_c^E$ are randomly allocated to users in $\mathcal{U}_s^c$ and $\mathcal{U}_{s,c}^E$, respectively. This strategy provides maximun fairness in terms of access opportunities to radio resources, but is unable to exploit the multiuser diversity gain. In contrast, the MC strategy selects the set of users maximizing the per-subcarrier capacity as,

$$\mathbf{u}_{MC} = \arg \max_{[u_1, \ \dots \ , u_K],} \sum_{i=1}^{K} C_{u_i}. \tag{3.38}$$
$$u_i \in \mathcal{U}_c,$$
$$u_i \neq u_j, \forall i \neq j$$

with K being the number of selected users. Note that the maximum capacity strategy implies the evaluation and computation of the sum-capacity for all possible user groupings and orderings. Even for moderate number of users, the exhaustive search is prohibitive in terms of computational complexity, thus, suboptimal user selection schemes must be devised. In this work a greedy algorithm based on the channel Frobenius norm will be

used for cell-edge cooperative users instead of the exhaustive search. The capacity of a MIMO channel is closely related to eigenvalues of the effective channel after pre-coding. For an accurate characterization of an user's channel capacity would be required more complex calculations like SVD would be required. A low complex alternative is the Frobenius norm; although it cannot exactly characterize the capacity, it provides an indication of the overall energy of the channel, being an appropriate indicator for the user selection. In particular, the technique used in this work is rooted on the algorithm introduced in [17].

The greedy algorithm used for the MC strategy is different for cell-center users and for Frequency Reuse 3 - noncooperative transmission. With those transmission schemes is going to be used another suboptimal algorithm [18]. In words, the algorithm first initializes a set $\mathcal{U}_{pool}$ containing all the potential users/modes (user and possible spatial modes transmitted) pairs over a subband. In the first iteration it selects the user/mode pair (m', α') providing the highest capacity, removes it from the set $\mathcal{U}_{pool}$, and updates the set of selected users with m' and the corresponding set of selected mode with α'. In the next iterations, and from the remaining unselected user/mode pairs in $\mathcal{U}_{pool}$, it finds the user/mode pair that provides the highest total capacity together with those already selected user/mode pairs. Note that the addition of a new user/mode pair modifies the null space of all the other users in the system and, hence, the zero multiuser interference constraint requirement may result in a decrease in the total utility. As a consequence, the algorithm terminates either when the number of allocated user/mode pairs reaches its maximum or when the total utility drops if more user/mode pairs are selected. The proposed algorithm needs to search over no more than $N_T|\mathcal{U}_c|N_R$ user/mode pairs, thus greatly reducing its complexity with respect to the exhaustive search method.

Note that these two scheduling policies provide two distinct alternatives in the capacity *vs.* fairness plane: while MC maximizes capacity at the cost of totally neglecting fairness, RR strives for fairness maximisation but neglecting any multiuser diversity gain. Any other scheduling policy (e.g., proportional fairness, exponential) will operate at an intermediate point of these two criteria.

TABLE 3.1: Simulation parameters

Parameters	Values
Number of cells	21
Number of sectors per cluster	3
Maximum transmit power per sector	40 W
Number of users per sector	N_u
Number of receive antennas per user	2
Number of transmit antennas per sector BS	2
Total bandwidth	$B = 7680$ kHz
Number of subcarriers	$N_{SC} = 512$
Subcarriers allocated to cell-edge users	$N_{SC}^{e} = 85$
Subcarriers allocated to cell-center users	$N_{SC}^{c} = 257$
Subcarrier bandwidth	$\Delta f = 15$ kHz
BS-to-BS distance	2 km
Standard deviation of shadowing	$\sigma_\beta = 6$
Shadowing correlation distance	50 m
Correlation between BS coefficient	0.5
Thermal noise density	-174 dBm/Hz
Noise Factor MS's antennas	7 dB

3.5 Simulation results

An OFDMA network with $N_c = 21$ cells is considered where up to three sector BSs cooperate to transmit to users in the cell edge, that is, $|\mathcal{B}_c| = 3$. Table 3.1 summarizes the rest of simulation parameters, with are in line with current 3GPP-LTE specifications [1].

3.5.1 Optimal Threshold SINR

The threshold SINR γ_{th} is a most critical parameter affecting the performance of any FFR-based system. In order to select a proper value for this parameter, it is important to study the impact the threshold has on the capacity measures for the different cooperation strategies. Figure 3.4 depicts a realization of the SINR measured in the network area, where the sectorization can be clearly appreciated. Figure 3.5 shows the capacity of cell center users as a function of γ_{th} and the number of $users/Km^2$ when using both greedy scheduling and RR scheduling. Given the antenna configuration for the cell centre ($M_E = 2$, $N_R = 2$), and the assumption that selected users are loaded with the maximum number of streams (i.e., N_R), it is clear that only one user per sector can be served in the central area on a given subcarrier. For the case of greedy scheduling,

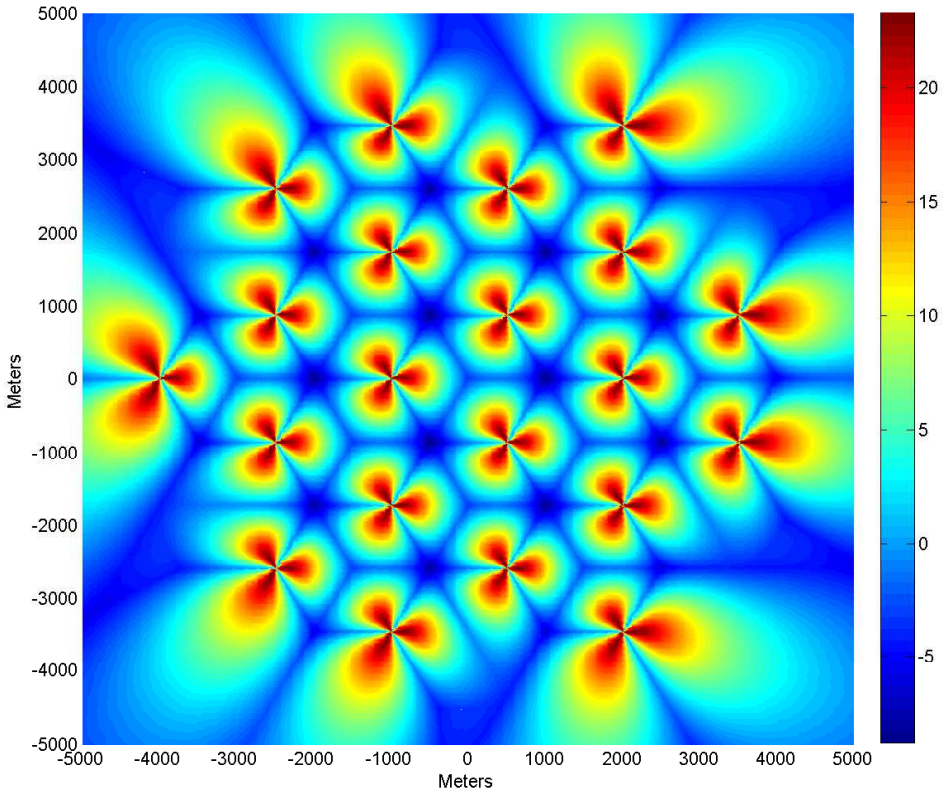

FIGURE 3.4: Measured SINR map.

when low user densities are considered, low values for SINR threshold γ_{th} tend to improve capacity. This effect is because lowering γ_{th} implies increasing the cell centre region, thus increasing the probability of finding one user with very strong SINR. Notice that when the user density grows, the optimum γ_{th} increases, which in turn implies a shrinkage of the central region. Obviously, as the curves indeed reveal, beyond a certain threshold SINR, the improvement is negligible as it is extremely unlikely to find a user so far away from the BS experiencing a large SINR. In fact, due to the gap between the greedy algorithms and the exhaustive search, for 20 $users/Km^2$ and 50 $users/Km^2$ a lower value of SINR threshold selection reduces the capacity. For the case of RR, there is a well defined optimum threshold that decreases with a decreasing number of active users in the cell. This effect is because the more users in the system, the higher the probability of finding users within a certain SINR threshold, thus increasing the optimum threshold value. Note that not having any cell-center user implies a waste of resources allocated to the cell-center area as these subcarriers will remain unassigned. In contrast, if a low SINR threshold is chosen, cell-center users close to the cell-edge area are likely to suffer

from large inter-cell interference. This effect can be appreciated when using RR as in this case these borderline users are still scheduled for transmission, thus lowering the average capacity (with an exhaustive search MC will almost completely neglect these users and they will rarely be allocated radio resources). This effect can be more clearly appreciated in figure 3.6 where the optimal value of γ_{th} maximizing the cell-center user capacity is shown as a function of the users in the network.

Figures 3.7 and 3.8 depicts the cell-edge users average capacity when using different CoMP and noncooperative schemes and schedulers for 20 $users/Km^2$. It can be deducted that if a lower γ_{th} is chosen, the probability that there are no cell-edge users increases, thus decreasing the corresponding capacity. On the contrary, a high γ_{th} almost guarantees the existence of cell-edge users, thus avoiding any waste of resources. It is very remarkable that the ZF-BD processing scheme achieves almost the same capacity than the more complex ZF-DPC-BD in MC scheduling. Furthermore, power allocation based on suboptimal solutions are effective in achieving almost the same capacity as the optimal solutions. SU-JT and SU-JT(suboptimal) can be seen to be the worst solution. As the fact they only serve one user ar a time, results in poor spectral efficiencies.

The radius selection should be done taking into account the capacity of both cell-center and cell-edge users. To this end, figures 3.9 and 3.10 shows how the overall average capacity varies as a function of the radius. Different transmission schemes and schedulers are tested when there are 20 $users/Km^2$. The results shows that $\gamma_{th} = 12dB$ is the optimal value in terms of capacity using RR strategy where as the optimum γ_{th} is in the range [10.5, 12] using MC strategy depending on the transmission technique employed. It can be observed that the cell-center users have greater influence than cell-edge users when choosing the optimal radius that maximize the overall average capacity of the system. As anticipated from the cell edge results, ZF-DPC-BD and ZF-BD with their suboptimal variations are the bests option; the performance of SU-JT and SU-JT(suboptim) have the worst result. For MC scheduling the JT-ZF seems to have a better performance with similar results to the rest of CoMP techniques. SU-JT and SU-JT(suboptimal) strategies result in the lowest throughput even lower than noncooperative schemes.

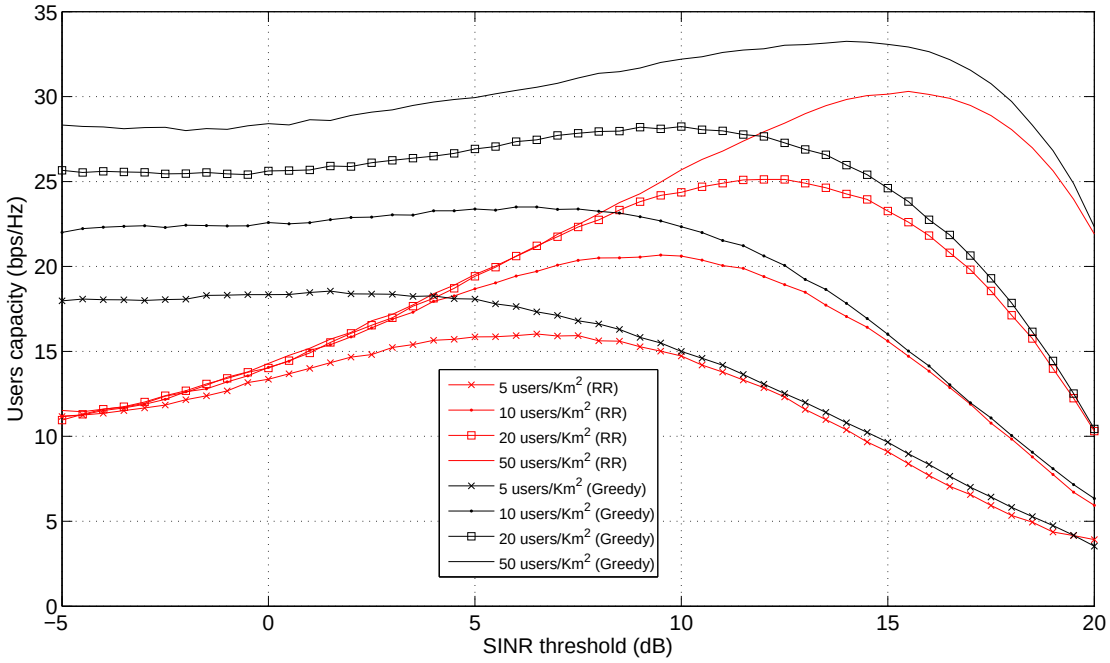

FIGURE 3.5: Cell-center user's spectral efficiency.

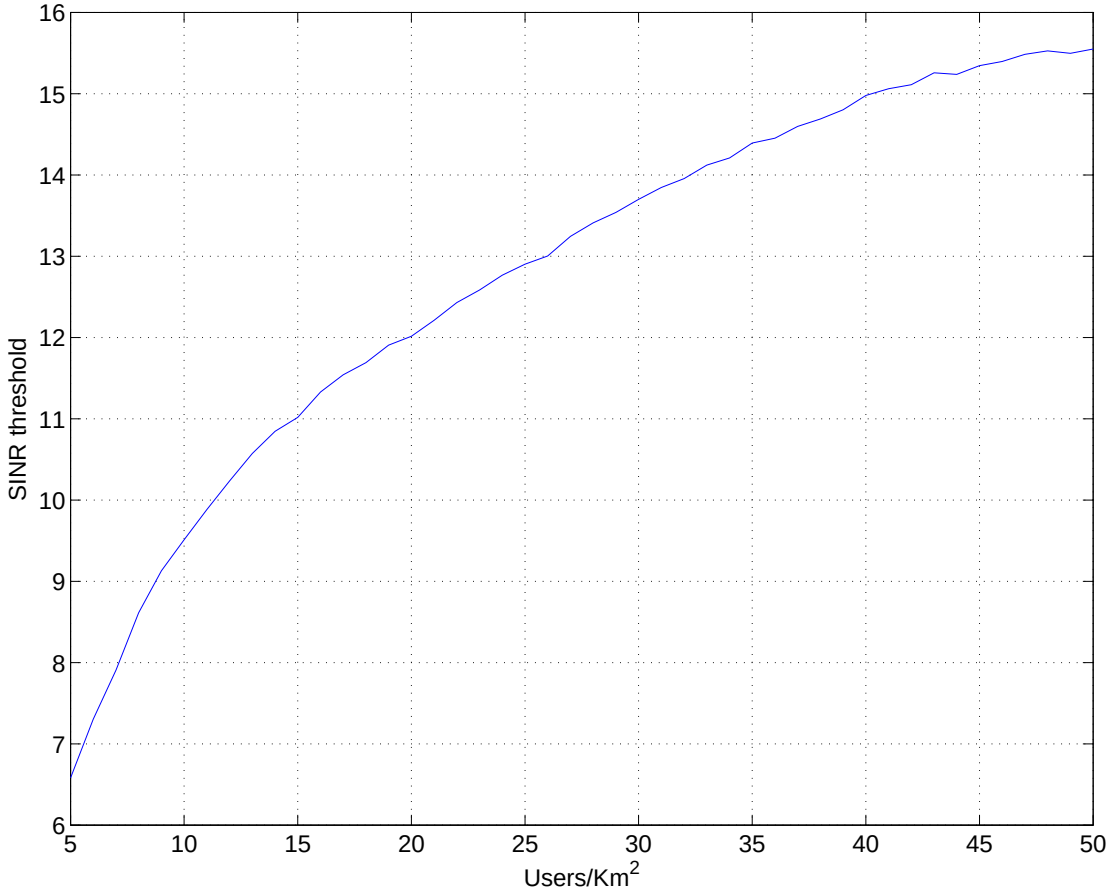

FIGURE 3.6: Optimum γ_{th} maximizing cell-center users' capacity for RR scheduling and MU-MIMO processing.

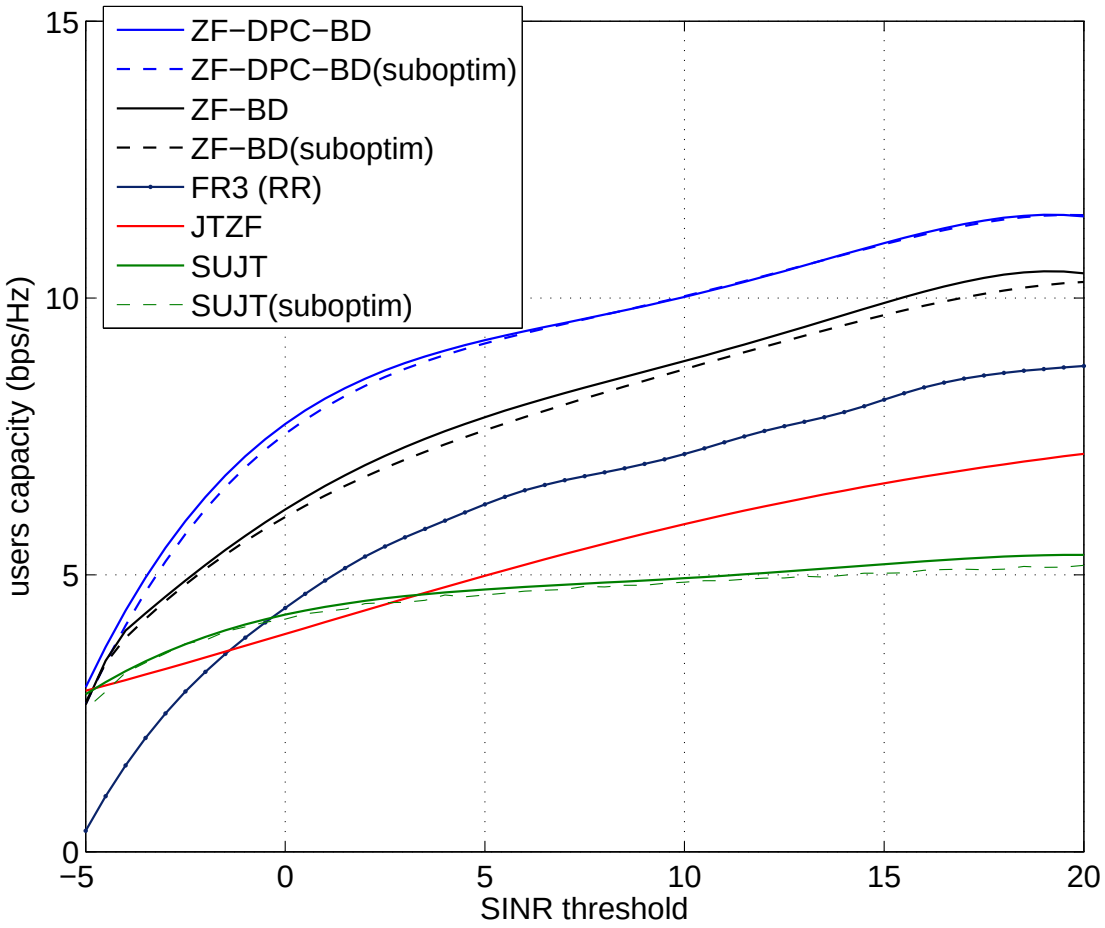

FIGURE 3.7: Cell-edge users capacity (RR).

3.5.2 Implementation considerations

It is worth nothing the different backhaul and complexity requirements of the different processing schemes applied on the edge and central regions. In particular, CoMP techniques require of a backhaul with enough capacity to support the exchange of user data and channel state information from all users that are being cooperatively served. Therefore, it is important to point out, and certainly a topic of interest for further work, that the definition of the centre and edge areas can also be influenced by this restriction: centre users do not imply any backhaul traffic whereas edge users do. In terms of complexity; JT-ZF, FR3 and suboptimal techniques are computationally simple and they rely on linear processing, unlike ZF-DPC-BD, ZF-BD and SU-JT where the optimization problem requires of complex subgradient algorithm. Additionally, ZF-DPC-BD requires complex non-linear processing to cancel the non-causal intra-cluster interference. In light of these remarks and the results presented so far, it seems that

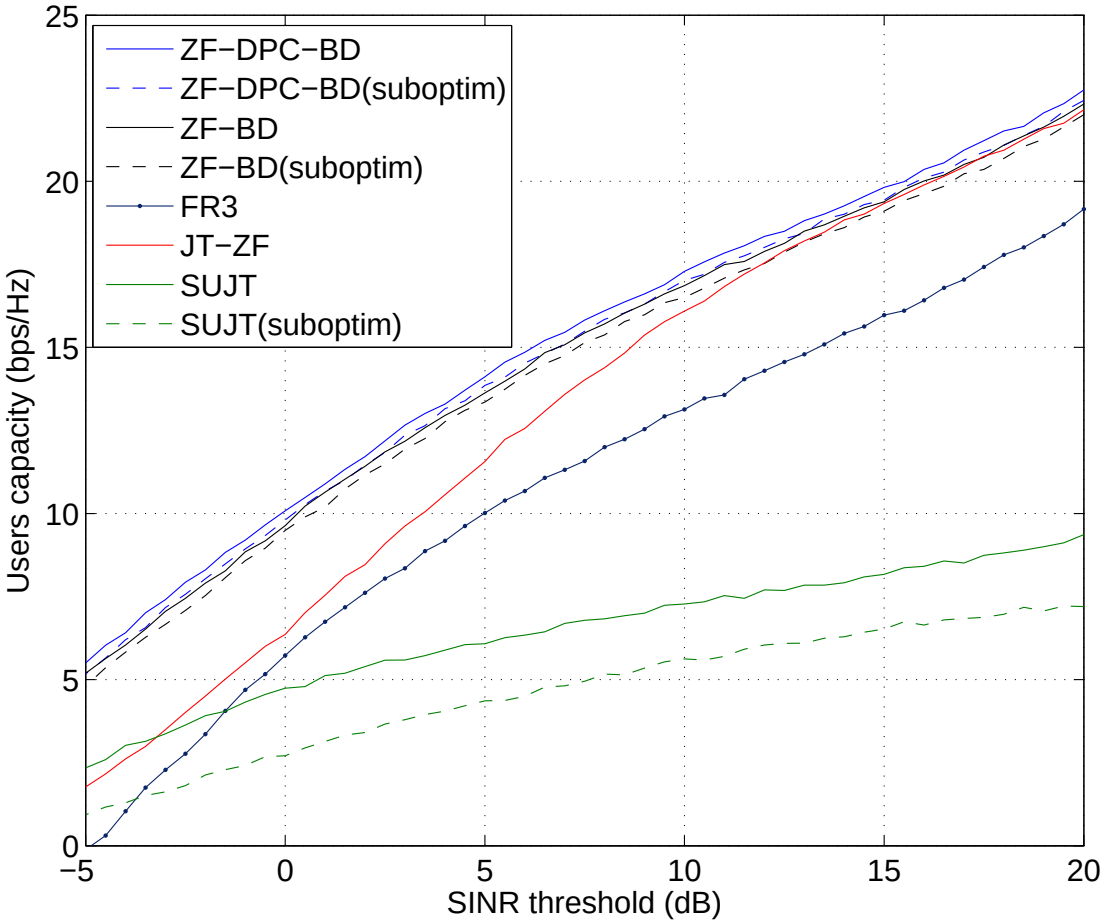

FIGURE 3.8: Cell-edge users capacity (Greedy).

suboptimal transmission represents an attractive trade-off in the capacity *vs* complexity plane while the use of MU-MIMO processing helps in increasing the overall capacity.

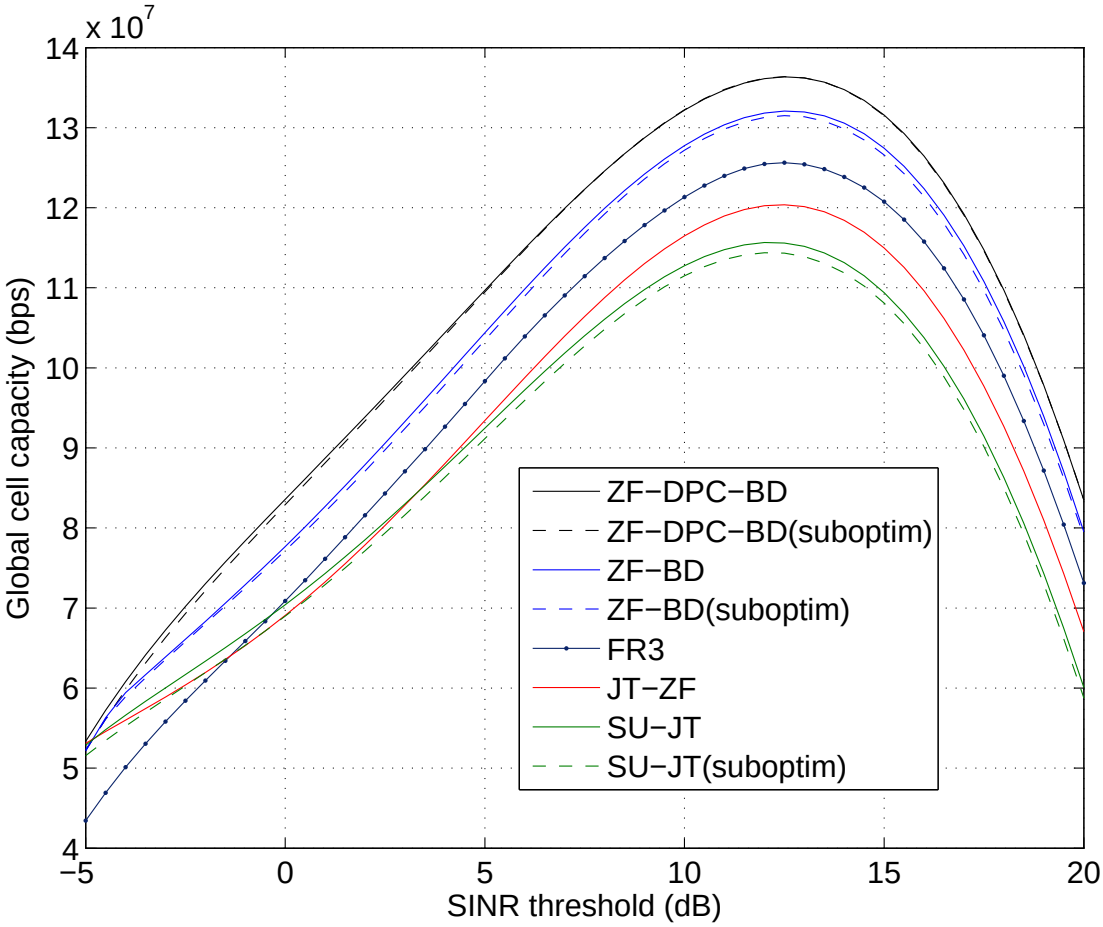

FIGURE 3.9: Overall cell capacity (RR).

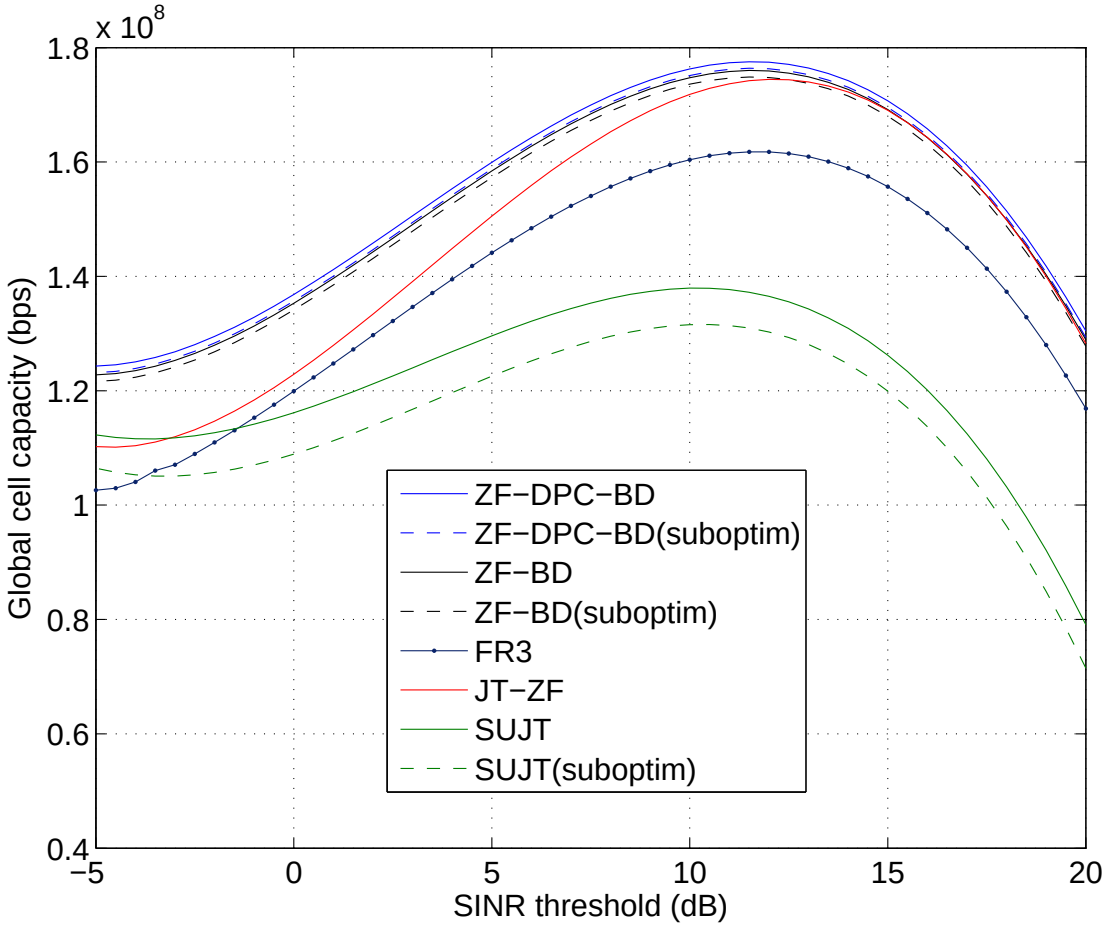

FIGURE 3.10: Overall cell capacity (Greedy).

Chapter 4

Conclusion and further work

This work has laid the ground for an FFR-aided OFDMA-based physical layer that combines advanced MIMO processing for both centre and edge users in the context of downlink LTE-A networks. SINR expressions are given for both types of users and models allowing the derivation of capacity bounds which in turn can serve as a useful metric to perform the resource allocation. The optimisation of the threshold SINR of the FFR reveals that this should be reduced as the number of users in the cell decreases approaching a value of around 15 dB that seems to be near-optimal when more than 35 users are in the system. Remarkably, the comparison among different CoMP processing schemes for the edge users demonstrate that the suboptimal architectures attains almost the same performance as the suboptimal schemes at a substantially lower computational cost for RR schemes.

Further work will progress along the following threads:

- Investigating Dynamic subcarrier assignments schemes in the FFR mechanism (cell-center o cell-edge) when combined with advanced MIMO processing.
- Derive resource management strategies in the form of subcarrier and power allocation, scheduling and transmission mode selection exploiting the PHY abstraction derived previously.

Bibliography

[1] H. Holma and A. Toskala. *LTE Advanced: 3GPP Solution for IMT-Advanced*. Wiley, 2012. ISBN 9781119974055.

[2] Zhikun Xu, G.Y. Li, Chenyang Yang, and Xiaolong Zhu. Throughput and optimal threshold for FFR schemes in OFDMA cellular networks. *Wireless Communications, IEEE Transactions on*, 11(8):2776–2785, 2012. ISSN 1536-1276. doi: 10.1109/TWC.2012.061912.110655.

[3] T.D. Novlan, R.K. Ganti, A. Ghosh, and J.G. Andrews. Analytical evaluation of fractional frequency reuse for OFDMA cellular networks. *Wireless Communications, IEEE Transactions on*, 10(12):4294–4305, 2011. ISSN 1536-1276. doi: 10.1109/TWC.2011.100611.110181.

[4] P. Marsch and G.P. Fettweis. *Coordinated Multi-Point in Mobile Communications: From Theory to Practice*. Coordinated Multi-point in Mobile Communications: From Theory to Practice. Cambridge University Press, 2011. ISBN 9781139502863.

[5] Q.H. Spencer, A.L. Swindlehurst, and M. Haardt. Zero-forcing methods for downlink spatial multiplexing in multiuser mimo channels. *Signal Processing, IEEE Transactions on*, 52(2):461–471, Feb 2004. ISSN 1053-587X. doi: 10.1109/TSP.2003.821107.

[6] G. Caire and S. Shamai. On the achievable throughput of a multiantenna gaussian broadcast channel. *Information Theory, IEEE Transactions on*, 49(7):1691–1706, July 2003. ISSN 0018-9448. doi: 10.1109/TIT.2003.813523.

[7] M. Assaad. Optimal fractional frequency reuse (FFR) in multicellular OFDMA system. In *Vehicular Technology Conference, 2008. VTC 2008-Fall. IEEE 68th*, pages 1–5, 2008. doi: 10.1109/VETECF.2008.381.

[8] Li-Chun Wang and Chu-Jung Yeh. 3-cell network MIMO architectures with sectorization and fractional frequency reuse. *Selected Areas in Communications, IEEE Journal on*, 29(6):1185–1199, 2011. ISSN 0733-8716. doi: 10.1109/JSAC.2011.110607.

[9] Young-Han Nam, Lingjia Liu, Yan Wang, C. Zhang, Joonyoung Cho, and Jin-Kyu Han. Cooperative communication technologies for LTE-advanced. In *Acoustics Speech and Signal Processing (ICASSP), 2010 IEEE International Conference on*, pages 5610–5613, 2010. doi: 10.1109/ICASSP.2010.5495250.

[10] M.K. Karakayali, G.J. Foschini, and R.A. Valenzuela. Network coordination for spectrally efficient communications in cellular systems. *Wireless Communications, IEEE*, 13(4):56–61, 2006. ISSN 1536-1284. doi: 10.1109/MWC.2006.1678166.

[11] G. Dimic and N.D. Sidiropoulos. On downlink beamforming with greedy user selection: performance analysis and a simple new algorithm. *Signal Processing, IEEE Transactions on*, 53(10):3857–3868, 2005. ISSN 1053-587X. doi: 10.1109/TSP.2005.855401.

[12] J.P. Romero. *Radio Resource Management Strategies in UMTS*. Wiley, 2005. ISBN 9780470022771. URL http://books.google.com.pr/books?id=0RcfAQAAIAAJ.

[13] J. Monserrat, R. Fraile, N. Cardona, and J. Gozalvez. Effect of shadowing correlation modeling on the system level performance of adaptive radio resource management techniques. In *Wireless Communication Systems, 2005. 2nd International Symposium on*, pages 460–464, Sept 2005. doi: 10.1109/ISWCS.2005.1547743.

[14] Rui Zhang. Cooperative multi-cell block diagonalization with per-base-station power constraints. In *Wireless Communications and Networking Conference (WCNC), 2010 IEEE*, pages 1–6, April 2010. doi: 10.1109/WCNC.2010.5506527.

[15] Robert G. Bland, Donald Goldfarb, and Michael J. Todd. The ellipsoid method: A survey. *Operations Research*, 29(6):pp. 1039–1091, 1981. ISSN 0030364X.

[16] Hongyuan Zhang and Huaiyu Dai. Cochannel interference mitigation and cooperative processing in downlink multicell multiuser mimo networks. *EURASIP Journal on Wireless Communications and Networking*, 2004(2): 202654, 2004. ISSN 1687-1499. doi: 10.1155/S1687147204406148. URL http://jwcn.eurasipjournals.com/content/2004/2/202654.

[17] Zukang Shen, Runhua Chen, J.G. Andrews, R.W. Heath, and B.L. Evans. Low complexity user selection algorithms for multiuser mimo systems with block diagonalization. In *Signals, Systems and Computers, 2005. Conference Record of the Thirty-Ninth Asilomar Conference on*, pages 628–632, Oct 2005. doi: 10.1109/ACSSC.2005.1599826.

[18] Guillem Femenias, Felip Riera-Palou, and Javier Pastor. Resource allocation in block diagonalization-based multiuser mimo-ofdma networks. In *Wireless Communications Systems (ISWCS), 2014 11th International Symposium on*, pages 411–417, Aug 2014. doi: 10.1109/ISWCS.2014.6933388.